RSC Advances

PAPER

View Article Online
View Journal | View Issue



Cite this: *RSC Adv.*, 2026, **16**, 20364

# Coumarin bearing triazole hybrids as cholinesterase inhibitors targeting Alzheimer's disease

Shahab Kermaninia,[a] Morteza Farnia,*[a] Mohammad Mahdavi[b] and Aida Iraji *[cd]

A series of novel coumarin-triazole hybrids (**12a–s**) were synthesized and evaluated for their inhibitory activities against cholinesterase including acetylcholinesterase (AChE) and butyrylcholinesterase (BChE), enzymes related to Alzheimer's disease. The structure–activity relationship (SAR) analysis revealed that substitutions at the 2-position of the aromatic ring significantly enhanced anti-BChE potency, with compound **12c** (2-fluorophenyl) exhibiting moderate activity with $IC_{50} = 4.37 \pm 0.91$ μM for BChE and $7.17 \pm 0.42$ μM for AChE. Docking studies demonstrated strong binding interactions of **12c** with critical residues in the active site of the enzyme. Molecular dynamics simulations confirmed the stability of the **12c**-AChE and **12c**-BChE complexes over 100 ns, with low RMSD values and stable hydrogen bonding. These findings highlight the importance of electronic and steric effects in optimizing cholinesterase inhibition and provide insights into the design of effective agents for Alzheimer's disease therapy.

Received 2nd December 2025
Accepted 19th February 2026

DOI: 10.1039/d5ra09311b

rsc.li/rsc-advances



## 1. Introduction

Alzheimer's disease (AD) is the leading cause of dementia, responsible for 60–80% of all cases. Given that age is the most well-known risk factor, AD poses a serious public health concern for the elderly. After the age of 65, the frequency of AD doubles every five years, and by the age of 85, almost one-third of people may have this disease.[1]

The global prevalence of AD is expected to rise dramatically with increasing life expectancy, placing an enormous burden on healthcare systems and societies. The primary symptoms of AD are memory loss, cognitive decline, and behavioral problems. AD progresses gradually, causing symptoms to worsen over time and ultimately making routine tasks more difficult.[2,3]

The disease is characterized by an accumulation of amyloid-beta plaques and neurofibrillary tangles in the brain, which lead to neuronal death. This neurodegeneration leads to brain atrophy, affecting memory and learning-related regions including the hippocampus and cerebral cortex.[4,5] Also, according to cholinergic dysfunction, the decline in acetylcholine, a neurotransmitter crucial for cognitive function, is a major feature of AD pathogenesis, which exacerbates cognitive function.[6]

Two key enzymes involved in acetylcholine metabolism are acetylcholinesterase (AChE) and butyrylcholinesterase (BChE). AChE hydrolyzes acetylcholine at the synaptic cleft, stopping cholinergic signaling. In Alzheimer's, there is a reduction in the level of acetylcholine due to cholinergic neuron loss, which plays a major role in memory impairment and cognitive decline. Inhibition of AChE can help increase the acetylcholine level, hence, supporting cognitive function.[7] Although acetylcholine is mainly broken by AChE, some studies indicate that BChE activity is increased in the brain of AD patients, particularly at the late stage of the disease. It was proposed that BChE contributes substantially to the remaining cholinergic activity and acetylcholine breakdown in advanced AD. As a result, pharmaceuticals that target both AChE and BChE have emerged to be effective strategies for enhancing cholinergic function and lowering cognitive deficits.[8]

Currently, there is no cure for AD, however, current medications try to reduce symptoms.[9] Despite extensive efforts, available drugs such as donepezil, rivastigmine, and galantamine offer only modest symptomatic relief without altering disease progression. As life expectancy increases globally, there is an urgent need for further research to develop more effective therapies for the elderly. Scientists have put enormous efforts in developing effective drugs to target this disease through developing cholinergic inhibitors.[10–12]

Coumarin-based compounds have attracted considerable attention as potential small-molecule candidates for AD therapy due to their diverse biological activities. Coumarin scaffold as synthetic and natural compounds is widely present in different structures as may possess neuroprotective, anti-oxidative, and AChE inhibitory potency, it is reported that owing to the

[a]*School of Chemistry, College of Science, University of Tehran, Tehran, Iran. E-mail: mfarnia@ut.ac.ir*

[b]*Endocrinology and Metabolism Research Center, Endocrinology and Metabolism Clinical Sciences Institute, Tehran University of Medical Sciences, Tehran, Iran*

[c]*Stem Cells Technology Research Center, Shiraz University of Medical Sciences, Shiraz, Iran. E-mail: iraji@sums.ac.ir; Fax: +98 713 230 2225; Tel: +98 713 230 3872*

[d]*Research Center for Traditional Medicine and History of Medicine, Department of Persian Medicine, School of Medicine, Shiraz University of Medical Sciences, Shiraz, Iran*

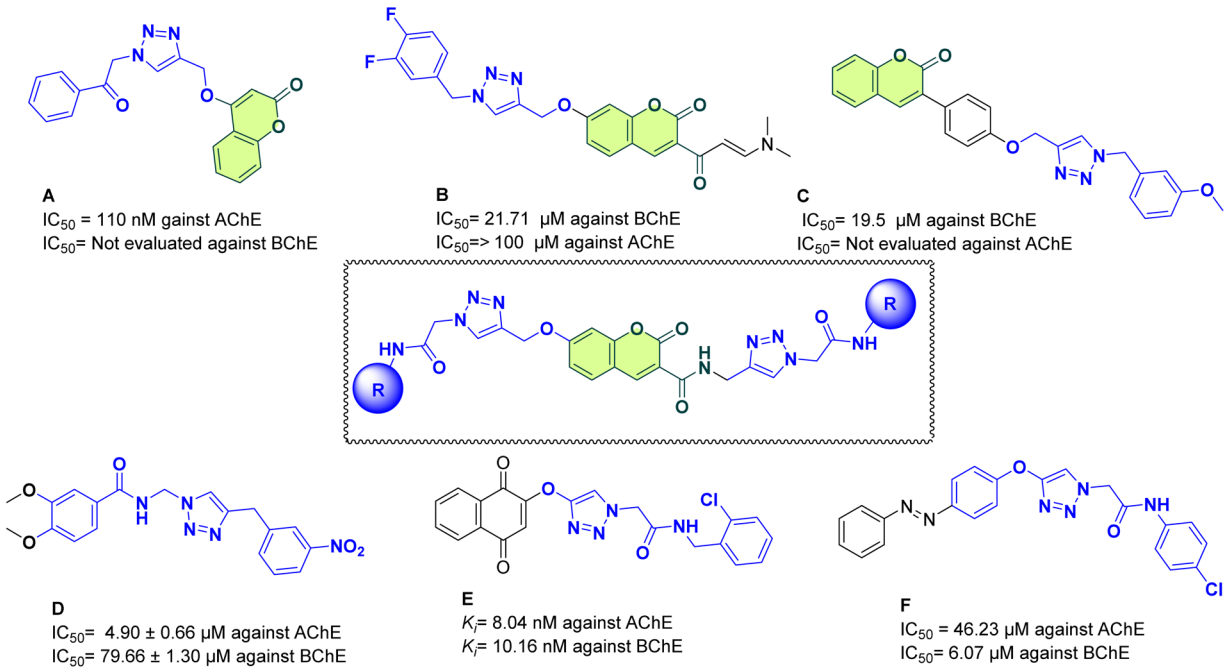


Fig. 1 Designing strategy.

presence of polar elements in the structure might facilitate better interaction with the biological target.[13,14] Bhagat *et al.*, in 2021, used a rational drug design approach, and a new series of coumarin or isatin scaffolds was developed. The AChE inhibitory activity showed that coumarin-1,2,3-triazole hybrids (compound **A**, Fig. 1) were noted to be more powerful inhibitors than isatin-1,2,3-triazole hybrids. Structure–activity relationship (SAR) studies revealed that also presence of an electronegative group such as F, Cl, or $NO_2$ on the substituted region improves AChE inhibition.[15] Likewise, 1,2,3-triazole-chromenone compounds (compound **B**) shown encouraging anti-AD effects, with an $IC_{50}$ of 21.71 μM against BChE and significant suppression of self-induced Aβ1–42 aggregation and AChE-induced Aβ aggregation (32.6% and 29.4%, respectively). According to SAR analysis, activity was increased by small-size halogen substituents.[16] The 1,2,3-triazole ring is a versatile scaffold with advantageous properties such as stability in both basic and acidic environments, excellent bioavailability, and low multidrug resistance.[17] Effective inhibition of AChE and BChE activities is made possible by its properties, which promote enzyme–inhibitor interactions. Docking studies have shown that triazole-based derivatives, including dimethylaminoacryloyl-chromenones (compound **C**), and aralkylamide (compound **D**) have strong anti-ChE activity, with van der Waals and hydrogen bonding interactions in the enzyme's active region being highlighted.[18–20]

Recent advancements include hybrid of triazoles such as 1,2,3-triazoles-naphthoquinone, where *ortho*-chlorine derivatives exhibited strong inhibitory activity. This derivative forms multiple interactions with the catalytic triad and the peripheral aromatic site (PAS) of the enzyme. Among the synthesized derivatives, compound **E**, featuring an *ortho*-chlorine moiety, exhibited the strongest inhibition of AChE and BChE, with $K_i$ values of 10.16 nM and 8.04 nM, respectively.[21] More recently, phenyl-diazenyl-phenoxy-1,2,3-triazole-acetamide (compound **F**) has emerged as a novel scaffold developed through the molecular hybridization of active pharmacophores. *In vitro* evaluations revealed that all newly synthesized compounds were more potent inhibitors of AChE and BChE than the standard drug galantamine. According to molecular docking experiments, the strongest compounds formed interactions with important elements of the AChE and BChE active sites, such as PAS and the catalytic active site (CAS).[22]

In this regard, the goal of the current work was to use molecular hybridization to develop new active molecules. A novel set of compounds with coumarin-triazole acetamide scaffold were designed, and synthesized, and their *in vitro* and *in silico* efficacy as possible anti-AD agents were assessed. A kinetic study was also conducted to learn more about the inhibitory mechanisms of the strongest analogs. *In silico* evaluations, such as molecular docking and molecular dynamics simulations, were carried out to predict and validate the binding interactions of these pharmaceuticals with their target enzymes to support the experimental results.

## 2. Results and discussion

### 2.1 Chemistry

A synthesis of triazole hybrids **12a–s** is exhibited in Fig. 2. Briefly, 2,4-dihydroxybenzaldehyde (compound **1**) was reacted *via* condensation with diethyl malonate (compound **2**) in the presence of piperidine to form a key compound **3**. Ethyl 7-hydroxy-2-oxo-2*H*-chromene-3-carboxylate (compound **3**) underwent propargylation using sodium hydride and propargyl bromide (compound **4**) in DMF at 80 °C, followed by precipitation and recrystallization from ethanol to produce the

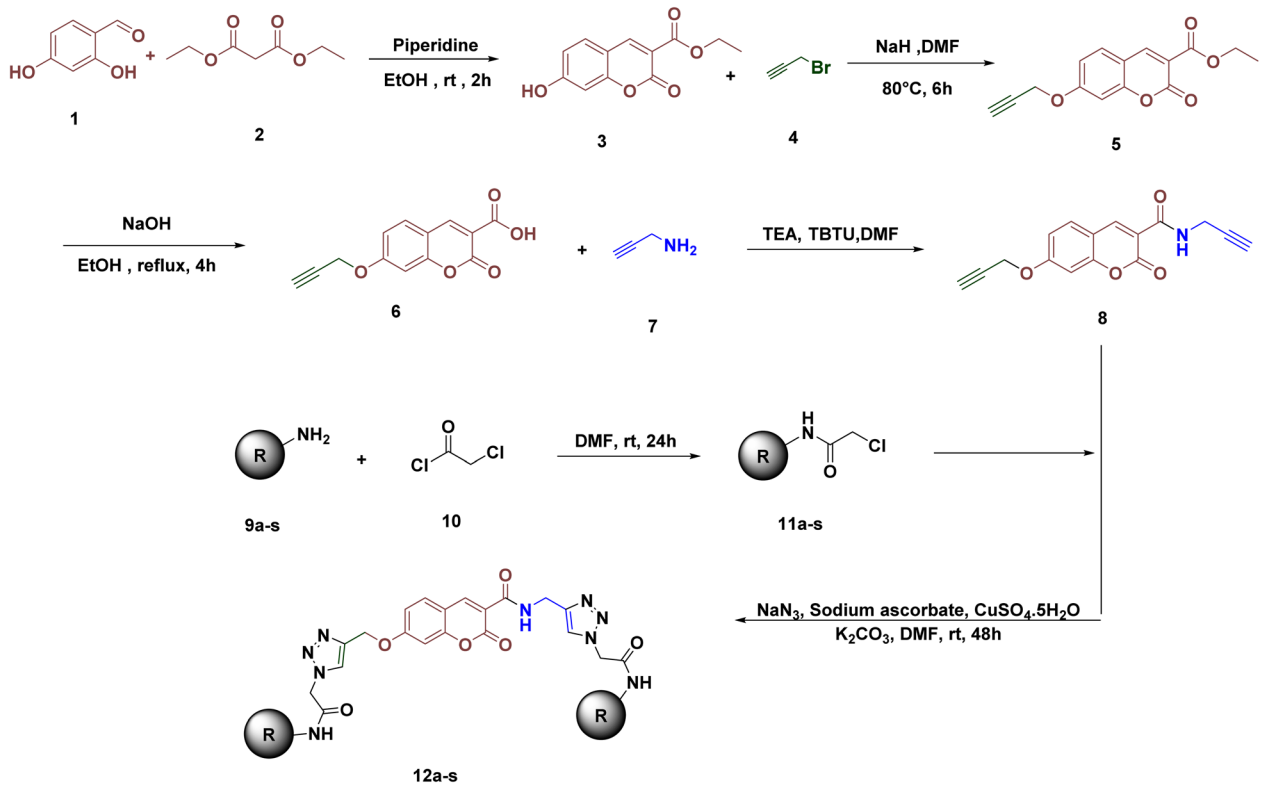


Fig. 2 Synthesis of 12a–s.

propargylated chromene derivative (compound **5**). The product was then hydrolyzed under reflux in a 1 : 1 ethanol : NaOH (5 M) solution at 100 °C, acidified and extracted using ethyl acetate to furnish the corresponding carboxylic acid derivative in excellent yield (compound **6**). Subsequently, the acid derivative (**6**) reacted with amine (**7**) in the presence of pyridine and in DMF to produce the carboxamide intermediate **8**. This intermediate is then reacted with 2-chloro-*N*-phenylacetamide (**11a–n**) in DMF, sodium azide, copper sulfate, and sodium ascorbate, using click chemistry at 40 °C for 48 h. The final triazole hybrids are obtained by filtering the reaction mixture and washing the solid with cold water/ethyl acetate, yielding pure triazole derivatives **12a–n**. The yields of the synthesized final products are presented in Table 1.

The structure of compound **12k** was confirmed by $^{1}$H and $^{13}$C NMR spectroscopy (Fig. 3). Two signals at 10.62 and 10.59 ppm were assigned to the amide N–H protons (H24, H41). The peak at 9.10 ppm, corresponding to the other amide N–H proton (H13), appeared as a triplet due to coupling with the adjacent $CH_2$ group. Two singlets at 8.33 and 8.88 ppm were attributed to the triazole C–H protons, confirming the successful formation of the 1,2,3-triazole rings. A singlet at 8.04 ppm was assigned to H10, which is located in the β-position relative to two carbonyl groups. The doublets at 7.94 and 7.31 ppm corresponded to H6 and H3, respectively, with H3 exhibiting a long-range coupling to H1. A doublet of doublets at 7.13 ppm was assigned to H1, which is coupled to both H3 and H6. Three singlet peaks at 5.31, 5.35, and 53.7 ppm were assigned to the three aliphatic $CH_2$ groups. The doublet at 4.61 ppm corresponded to the $CH_2$ adjacent to the amide N–H. In the $^{13}$C NMR spectrum, the most

Table 1 Yields of the synthesized derivatives

| Compounds | Yield% | Compounds | Yield% | Compounds | Yield% |
|---|---|---|---|---|---|
| **12a** | 67 | **12h** | 68 | **12n** | 74 |
| **12b** | 78 | **12i** | 77 | **12o** | 75 |
| **12c** | 65 | **12j** | 74 | **12p** | 73 |
| **12d** | 61 | **12k** | 68 | **12q** | 66 |
| **12e** | 71 | **12l** | 72 | **12r** | 73 |
| **12f** | 63 | **12m** | 75 | **12s** | 71 |
| **12g** | 79 | | | | |

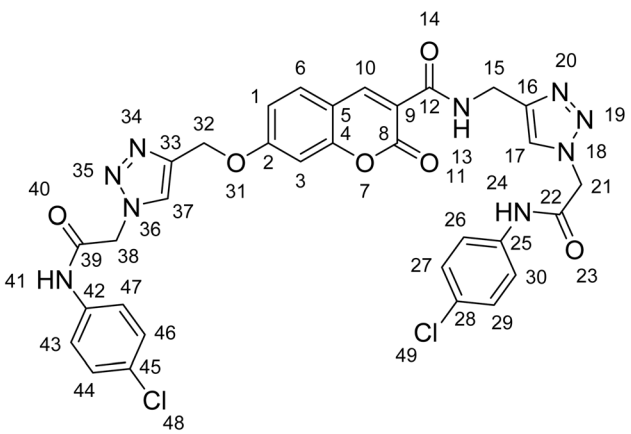

Fig. 3 Chemical structure of 12k.

Table 2 BChE and AChE inhibitory activities of **12a–n**[a]

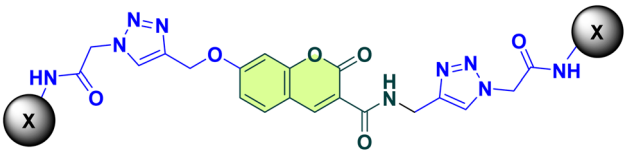

| Compound | R | AChE | | BChE | |
|---|---|---|---|---|---|
| | | % Inhibition at 50 μM | $IC_{50}$ (μM) | % Inhibition at 50 μM | $IC_{50}$ (μM) |
| **12a** | Phenyl | 84.43 ± 6.56 | 23.06 ± 3.74 | 46.02 ± 0.41 | >50 |
| **12b** | 2-Methylphenyl | 52.59 ± 2.14 | 38.46 ± 0.63 | 56.19 ± 2.32 | 10.07 ± 1.63 |
| **12c** | 2-Fluorophenyl | 62.03 ± 2.36 | 7.17 ± 0.42 | 66.66 ± 0.05 | 4.37 ± 0.91 |
| **12d** | 2-Chlorophenyl | 33.92 ± 4.19 | >50 | 54.71 ± 3.15 | 39.90 ± 3.89 |
| **12e** | 3-Methylphenyl | 24.58 ± 1.47 | >50 | 24.15 ± 2.63 | >50 |
| **12f** | 3-Chlorophenyl | 37.35 ± 3.52 | >50 | 45.65 ± 0.55 | >50 |
| **12g** | 4-Methylphenyl | 15.73 ± 3.39 | >50 | 37.98 ± 1.63 | >50 |
| **12h** | 4-Ethylphenyl | 16.44 ± 1.94 | >50 | 39.29 ± 1.13 | >50 |
| **12i** | 4-Methoxyphenyl | 32.23 ± 1.48 | >50 | 24.58 ± 3.36 | >50 |
| **12j** | 4-Fluorophenyl | 37.11 ± 3.02 | >50 | 32.19 ± 2.93 | >50 |
| **12k** | 4-Chlorophenyl | 44.03 ± 6.83 | >50 | 43.89 ± 7.41 | >50 |
| **12l** | 4-Bromophenyl | 21.75 ± 5.11 | >50 | 39.38 ± 7.12 | >50 |
| **12m** | 4-Trifluoromethylphenyl | 19.33 ± 1.89 | >50 | 38.78 ± 9.52 | >50 |
| **12n** | 2,4-Dimethylphenyl | 59.65 ± 1.77 | 6.65 ± 1.31 | 54.33 ± 2.46 | 17.07 ± 4.61 |
| **12o** | 2,4-Dimethoxyphenyl | 52.53 ± 0.64 | 18.66 ± 1.82 | 58.37 ± 5.42 | 17.28 ± 0.70 |
| **12p** | 3,4,5-Trimethoxyphenyl | 22.87 ± 2.36 | >50 | 35.14 ± 2.46 | >50 |
| **12q** | Benzyl | 56.24 ± 6.73 | 34.57 ± 15.74 | 47.50 ± 1.03 | >50 |
| **12r** | 4-Methylbenzyl | 54.53 ± 2.24 | 46.68 ± 0.89 | 10.49 ± 0.55 | >50 |
| **12s** | Phenylethyl | 24.70 ± 3.24 | >50 | 30.26 ± 2.41 | >50 |

[a] Donepezil as positive control showed $IC_{50}$ = 10.6 ± 2.1 μM against BChE and $IC_{50}$ = 0.079 ± 0.05 μM against AChE.

downfield signals were attributed to the two carbonyl moieties located at the termini of the molecular structure (C22, C39). The following four signals were assigned to four quaternary carbons directly attached to oxygen atoms. Two sets of high-intensity peaks appearing at $\delta$ 121 and 129 ppm corresponded to the aromatic carbon atoms C26, C27, C29, C30, C43, C44, C46, and C47. The most upfield signal in the aromatic region was assigned to carbon C3, due to the negative charge generated in resonance structures involving the adjacent oxygen atoms. The most upfield signal overall was assigned to carbon C15, which is directly bonded to the amide nitrogen. The most deshielded signal in the aliphatic region was assigned to carbon C32, which is directly bonded to an oxygen atom. Finally, two closely spaced signals observed at approximately 52 ppm were assigned to carbons C21 and C38.

### 2.2 AChE inhibitory activity

The relationship between structural modifications and biological activity against AChE was studied (Table 2).

The unsubstituted analog (compound **12a**) exhibited moderate activity, with an $IC_{50}$ of 23.06 ± 3.74 μM. Substituents at various positions on the aromatic ring had significant effects on the potency against AChE. Substituents at the 2-position showed mixed effects depending on their electronic properties. For example, compound **12c** (2-fluorophenyl) demonstrated the most potent activity, with an $IC_{50}$ of 7.17 ± 0.42 μM, highlighting the benefit of a small electron-withdrawing fluorine group. Conversely, bulkier groups such as chlorine (compound **12d**) reduced activity, suggesting that steric hindrance may weaken enzyme interaction.

Substituents at the 3-position also resulted in weak activity. For instance, compounds **12e** (3-methylphenyl) and **12f** (3-chlorophenyl) exhibit significantly lower potency than the unsubstituted compound.

Most compounds exhibited moderate to weak activity for derivatives with substituents at the 4-position. Compound **12k** (4-chlorophenyl) showed % inhibition of 44.03 ± 6.83, while compound **12g** (4-methylphenyl), **12h** (4-ethylphenyl), **12l** (R: 4-bromophenyl) and **12m** (R: 4-trifluoromethylphenyl) displayed even lower activity, with % inhibition values of 15.73 ± 3.39, 16.44 ± 1.94, 21.75 ± 5.11, and 19.33 ± 1.89, respectively. Also, **12i** and **12j** exhibited around 30% inhibition at 50 μM. These results suggest that the 4-position is less favorable for enhancing potency, regardless of substituent electronic or steric properties.

Disubstituted compounds demonstrated significant activity, influenced by the combination of substituents. Compound **12n** (2,4-dimethylphenyl) exhibited the strongest activity, with an $IC_{50}$ of 6.65 ± 1.31 μM, indicating that dual methyl substitution enhances binding affinity. Similarly, compound **12o** (2,4-dimethoxyphenyl) showed an $IC_{50}$ of 18.66 ± 1.82 μM,

highlighting the favorable effects of electron-donating groups. These results indicate that 2,4-disubstitution is a favorable strategy for AChE inhibition.

The trisubstituted derivative compound **12p** (3,4,5-trimethoxyphenyl) exhibited weak activity, with % inhibition of 22.87 ± 2.36, likely due to excessive steric hindrance and the reduced ability to interact effectively with the enzyme active site. Replacing the phenyl group with a benzyl group (compound **12q**) showed moderate activity ($IC_{50}$ = 34.57 ± 15.74 μM), but no significant improvement was observed compared with **12a**. However, **12r** bearing 4-methylbenzyl showed $IC_{50}$ = 46.68 ± 0.89 μM, which showed improvement *vs.* **12g**.

In summary, the most potent inhibitors were compound **12c** (2-fluorophenyl) and compound **12n** (2,4-dimethylphenyl), which demonstrated strong activity due to favorable steric and electronic effects. Substituents at the 2-position generally improved potency, while those at the 3- and 4-positions showed limited or no enhancement. These findings underscore the importance of substituent type and position for optimizing AChE inhibition in AD studies.

### 2.3 BChE inhibitory activity

The relationship between structural modifications and biological activity against BChE was analyzed based on $IC_{50}$ values and % inhibition at 50 μM. The unsubstituted analog (compound **12a**) exhibited 46.02% inhibition at 50 μM, indicating moderate activity. To enhance potency, various substituents were introduced at different positions on the phenyl ring, which significantly influenced biological activity (Table 2).

Substituents at the 2-position generally improved potency. For example, compound **12b** (R = 2-methylphenyl), with an electron-donating group, exhibited an $IC_{50}$ of 10.07 ± 1.63 μM, indicating significant improvement over the unsubstituted compound. The most potent compound was compound **12c** (R = 2-fluorophenyl), with an $IC_{50}$ of 4.37 ± 0.91 μM, highlighting the effectiveness of a small electron-withdrawing fluorine group at this position. However, replacing the small fluorine group with bulkier groups like chlorine (compound **12d**) reduced the potency. This suggests that steric hindrance diminishes the benefits of larger substituents.

Changing the chlorine position from the 2- to the 3-position significantly reduced potency to 45.65% inhibition at 50 μM *vs.* compound **12d** exhibited an $IC_{50}$ of 39.90 ± 3.89 μM for **12f**. Similarly, 3-methylphenyl substitution (compound **12e**) decreases potency relative to **12b**. This observation highlights the destructive role of *meta* substituent position for activity.

Substituents at the 4-position exhibited moderate to low activity across all derivatives (compounds **12g–m**), with no significant differences among them. This suggests that substituents at this position have a limited impact on potency, regardless of their electronic or steric properties.

Disubstituted derivatives also exhibited improved potency, as shown by compounds **12n** (2,4-dimethylphenyl) and **12o** (2,4-dimethoxyphenyl), with $IC_{50}$ values of 17.07 ± 4.61 μM and 17.28 ± 0.70 μM, respectively.

The trisubstituted derivative compound **12p** (3,4,5-trimethoxyphenyl) exhibited weak activity, with % inhibition of 35.14%, suggesting that excessive steric bulk impair binding and inhibitory activity. Replacing the phenyl group with a benzyl one (compound **12q**) showed no significant improvement in potency *vs.* **12a**, indicating that extending the aromatic system does not enhance activity. The same trend were seen in **12r** *vs.* **12g** in which elongation of the linker is not favorable.

Overall, substituents at the 2-position generally improved inhibition, with small electron-withdrawing groups such as fluorine showing the greatest potency. Steric hindrance and electron-donating groups, especially in other positions, tend to reduce activity. These findings underscore the importance of optimizing substituent position for developing potent BChE inhibitors.

### 2.4 Kinetic studies of 12c

The kinetics of BChE inhibition by compound **12c** were investigated at various inhibitor concentrations. Different concentrations of the substrates butyrylthiocholine iodide (BTCI) were

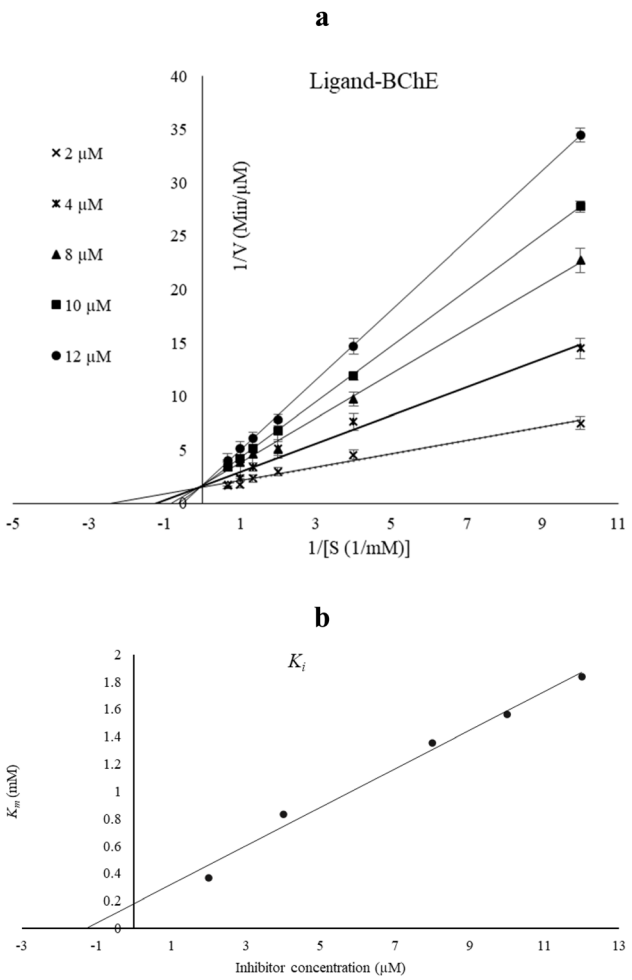


Fig. 4 (a) Lineweaver–Burk plot for the inhibition of BChE by **12c** in the presence of various concentrations of the substrate. (b) Secondary plot for the calculation of the inhibition constant of compound **12c**.

Table 3 Molecular docking study of **12a–s** against AChE and BChE

| | AChE | | BChE | |
|---|---|---|---|---|
| Compound | Type of interaction with residue | Binding energy | Type of interaction with residue | Binding energy |
| **12a** | H-bond Phe295<br>π–π stacking Tyr341<br>H-bond Tyr124<br>π–π stacking Tyr124<br>H-bond Tyr133<br>π–π stacking Trp86<br>π–π stacking Trp286 | −14.40 | H-bond Ser287<br>H-bond Thr284<br>π-cation His438<br>π–π stacking Tyr332 | −9.085 |
| **12b** | H-bond Glu292<br>H-bond Phe295<br>H-bond Arg296<br>π–π stacking Phe337<br>π–π stacking Phe338<br>π–π stacking Tyr341<br>π–π stacking Trp286 | −11.143 | H-bond Gly197<br>2 × π–π stacking Trp82<br>H-bond Pro285 | −10.804 |
| **12c** | H-bond Glu292<br>H-bond Phe295<br>H-bond Arg296<br>H-bond Tyr124<br>π–π stacking Tyr341<br>π–π stacking Phe338<br>π-cation interaction His447 | −13.678 | H-bond Asp70<br>H-bond Asn68<br>H-bond Glu197<br>π–π stacking Tyr332<br>2 × π–π stacking Trp82 | −11.443 |
| **12d** | Halogen bond Asp74<br>π–π stacking Tyr341<br>π–π stacking Phe338<br>π–π stacking Trp285<br>H-bond Glu292 | −10.828 | Halogen bond Gly197<br>H-bond Gly197<br>π–π stacking Phe329<br>H-bond Pro285<br>H-bond Tyr284 | −10.813 |
| **12e** | H-bond Tyr124<br>H-bond Leu289<br>π–π stacking Trp86<br>π–π stacking Tyr341 | −9.342 | H-bond Thr284<br>H-bond Asn289 | −10.051 |
| **12f** | Halogen bond Gln71<br>Halogen bond Val73<br>π–π stacking Trp286 | −9.817 | Halogen bond Thr122<br>π-cation His438<br>2 × π–π stacking Tyr332<br>H-bond Ser287 | −9.847 |
| **12g** | H-bond Tyr341<br>2 × π–π stacking Trp286<br>π–π stacking Val340 | −10.858 | H-bond Gly116<br>H-bond Ser198<br>H-bond Ser287 | −9.107 |
| **12h** | H-bond Tyr341<br>2 × π–π stacking Tyr341<br>π–π stacking Phe338<br>2 × π–π stacking Trp86 | −8.212 | H-bond Ser72<br>H-bond Gly116<br>π–π stacking Tyr332<br>π–π stacking Phe329 | −9.732 |
| **12i** | H-bond Tyr124<br>H-bond Asp74<br>π–π stacking Tyr124<br>π–π stacking Tyr341<br>π–π stacking Tyr72 | −9.727 | H-bond Asn68<br>π–π stacking Tyr332<br>2 × π–π stacking Phe329 | −8.218 |
| **12j** | π–π stacking His287<br>π–π stacking Tyr124<br>π–π stacking Tyr341<br>H-bond Tyr124<br>π–π stacking Tyr337 | −9.865 | π–π stacking Trp82<br>π–π stacking Phe329<br>π–π stacking Tyr332<br>H-bond Asn68<br>H-bond Gln119 | −9.703 |
| **12k** | π–π stacking Tyr341<br>H-bond Trp341<br>H-bond Phe295<br>π–π stacking Tyr337 | −9.410 | Halogen bond Asp70<br>H-bond Tyr128<br>π–π stacking Trp82<br>π–π stacking Tyr332 | −10.213 |
| **12l** | Halogen bond Asp74<br>π–π stacking His447<br>π–π stacking Tyr124<br>π–π stacking Trp286<br>π–π stacking Trp341 | −9.995 | Halogen bond Tyr128<br>π–π stacking Trp82<br>π–π stacking Tyr332 | −9.044 |
| **12m** | 2 × π–π stacking Tyr341 | −9.467 | H-bond Asp70 | −10.946 |

Table 3 (*Contd.*)

| Compound | AChE | | BChE | |
|---|---|---|---|---|
| | Type of interaction with residue | Binding energy | Type of interaction with residue | Binding energy |
| | H-bond Tyr124 | | H-bond Ser72<br>π–π stacking Trp82 | |
| **12n** | H-bond Glu292<br>H-bond Phe295<br>H-bond Arg296<br>π–π stacking Tyr337<br>π–π stacking Tyr341<br>π–π stacking Trp86 | −14.390 | H-bond Thr284<br>H-bond Ser287<br>π-cation His438 | −10.169 |
| **12o** | 2 × H-bond Tyr124<br>π–π stacking Tyr124<br>π–π stacking Tyr341<br>π–π stacking Trp86<br>π–π stacking Trp286 | −10.820 | H-bond Ser287<br>H-bond Thr284<br>π-cation His438<br>π–π stacking Tyr332 | −9.085 |
| **12p** | 2 × π–π stacking Tyr341<br>π–π stacking Phe338 | −7.138 | H-bond Gly197<br>2 × π–π stacking Trp82<br>H-bond Pro285 | −10.804 |
| **12q** | π–π stacking Trp286<br>2 × H-bond Glu292<br>π–π stacking Tyr341<br>π–π stacking Tyr337 | −12.514 | H-bond Asp70<br>H-bond Asn68<br>H-bond Glu197<br>π–π stacking Tyr332<br>2 × π–π stacking Trp82 | −11.443 |
| **12r** | π–π stacking Trp86<br>H-bond Asp74<br>H-bond Gly202<br>H-bond Phe295 | −12.514 | H-bond Thr230<br>H-bond Tyr128 | −9.443 |
| **12s** | H-bond Gly202<br>π–π stacking Trp286<br>π–π stacking Tyr341 | −9.245 | π–π stacking Tyr82<br>H-bond Ser287 | −8.085 |

used to determine initial velocity values. The reciprocal of the substrate concentration (1/[S]) was plotted against the reciprocal of the initial velocity (1/*V*) to generate Lineweaver–Burk plots.

For BChE (Fig. 4a), the Lineweaver–Burk plot showed that both the slope and *y*-intercept increased with increasing inhibitor concentrations, indicating a competitive mode of inhibition. The inhibition constant ($K_i$) for compound **12c** was determined from the secondary plot (Fig. 4b) and found to be 2.05 μM.

### 2.5 Molecular docking studies

Molecular docking studies were conducted to investigate the behavior of the target compound within the AChE and BChE binding sites. First redocking of the crystallographic inhibitor were peromed and RMSD between the docked and experimental

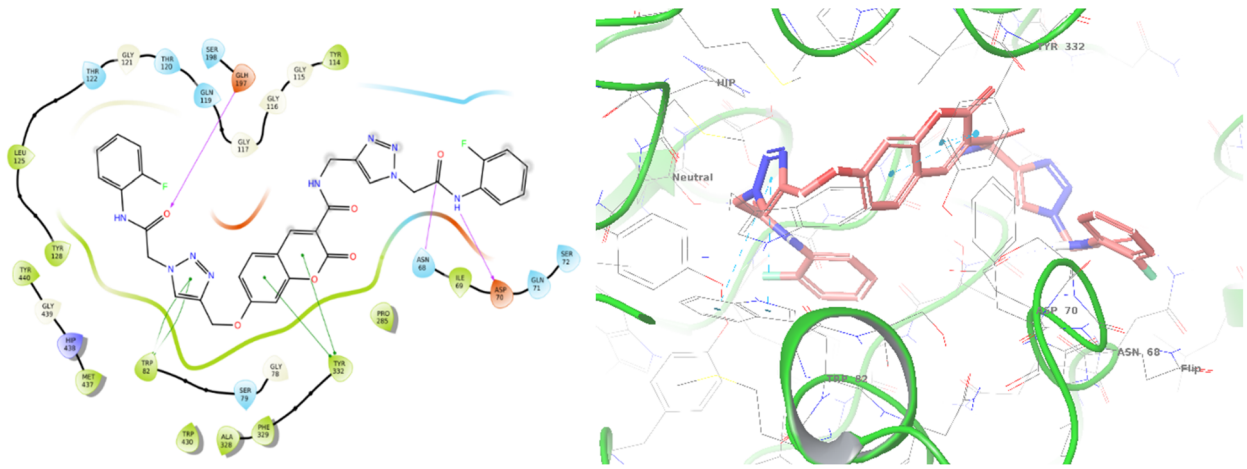


Fig. 5 Proposed binding mode for compound **12c** docked at the active site of BChE.

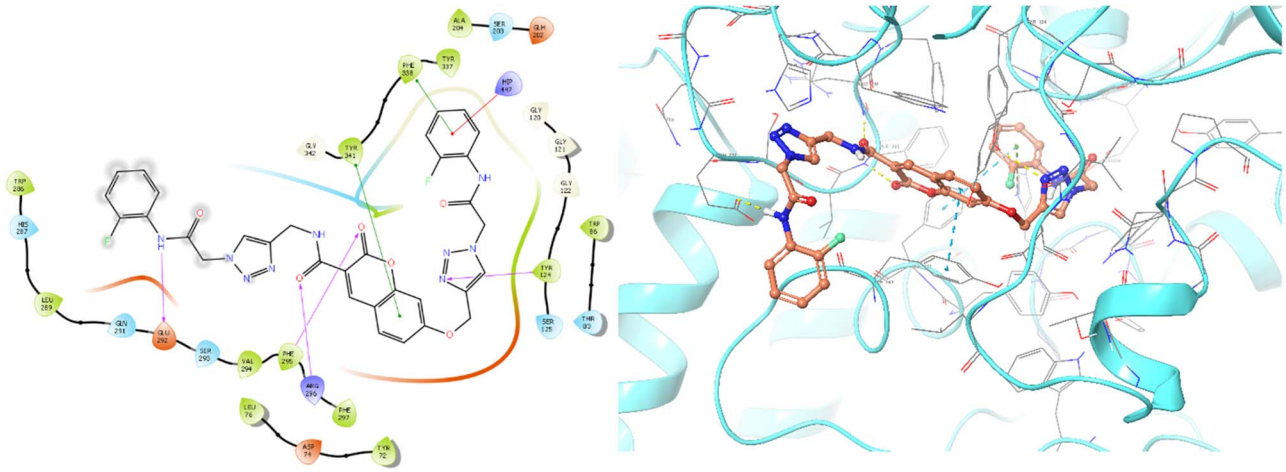

Fig. 6 Proposed binding mode for compound **12c** docked at the active site of AChE.

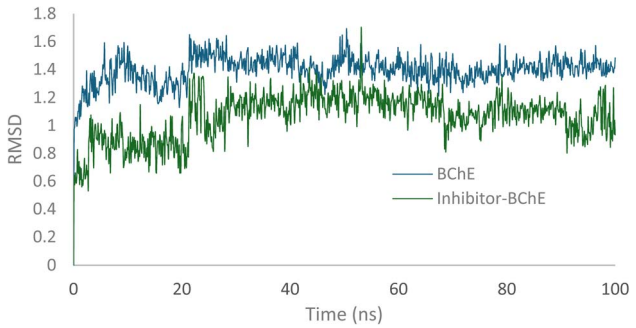


Fig. 7 RMSD of BChE *vs.* **12c**-BChE.

poses was found to be less than 2 Å, confirming the reliability of the docking procedure.

The detailed molecular docking (Table 3) and enzyme inhibition data (Table 2) provide clear evidence of the structural features required for effective AChE inhibition. Compounds **12a**, **12c**, and **12n** emerged as the most potent inhibitors with $IC_{50}$ values of 23.06 μM, 7.17 μM, and 6.65 μM, respectively, and docking scores of −14.40, −13.68, and −14.39 kcal $mol^{-1}$. The active molecules show a consistent formation of π–π stacking interactions with Trp86 (located in the choline-binding site) and Trp286 (located in the PAS), as well as significant hydrogen bonding with Glu292, Phe295, and Arg296. The combined interactions seem to be important for achieving high binding affinity and potent inhibitory activity. Compound **12c** showed a π-cation interaction with His447, a key residue within the catalytic triad of AChE. This interaction with the catalytic triad is may contribute to superior inhibitory potency compared to other analogs. Compounds **12a** and **12n**, while still potent, are stabilized mainly by the interactions with the choline-binding site and PAS, without directly targeting the catalytic triad. In contrast, less active or inactive derivatives (such as compounds **12d**, **12e**, **12f**, **12g**, **12h** and **12i**) mostly showed significantly higher docking energies (less favorable binding scores), which correlated with their lower enzyme inhibition percentages.

The comparative examination of BChE docking scores and molecular interactions reveals striking features accounting for significant increases in activity. The most potent derivatives seem to include **12c** ($IC_{50}$ = 4.37 μM, binding energy: −11.443 kcal $mol^{-1}$), **12b** ($IC_{50}$ = 10.07 μM, −10.804 kcal $mol^{-1}$), **12n** ($IC_{50}$ = 17.07 μM, −10.169 kcal $mol^{-1}$), and **12o** ($IC_{50}$ = 17.28 μM, −10.685 kcal $mol^{-1}$), as they showed much stronger docking scores than the less active analogs who had mostly binding energies between −9.0 and −10.2 kcal $mol^{-1}$. Most importantly, these potent compounds appeared to form multiple hydrogen bonds with critical residues of Gly197, Glu197, Asn68, Pro285,

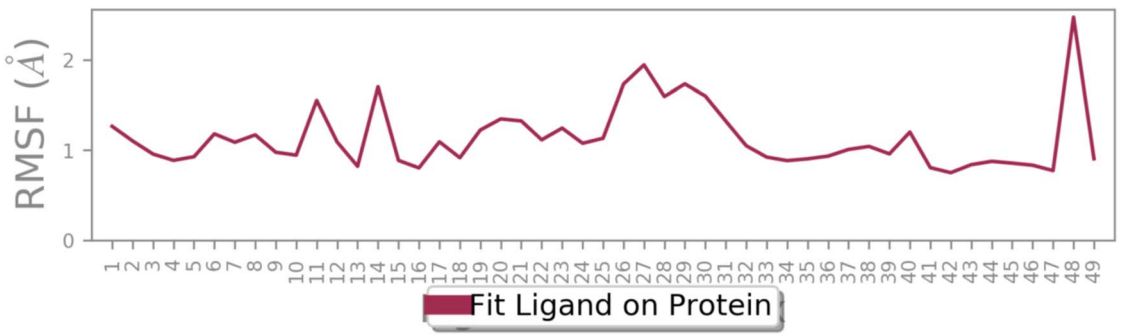


Fig. 8 RMSD of **12c** in the active site of BChE.

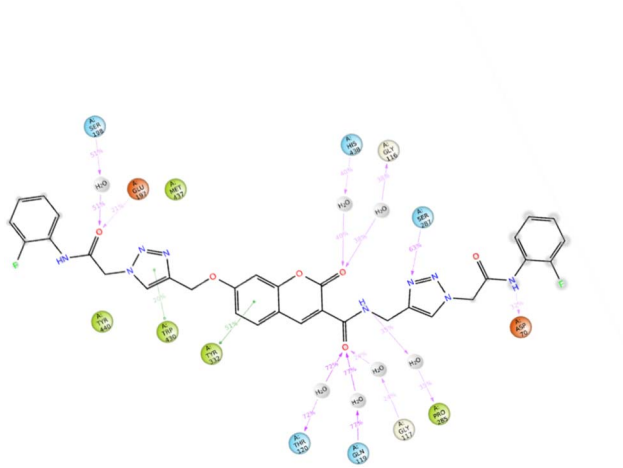

Fig. 9 A schematic of detailed **12c** atom interactions with the protein residues. Interactions that occur more than 20.0% of the simulation time in the selected trajectory.

and Thr284, and Ser287. Interestingly, the hydrogen bonding with Gly197 was common with active compounds **12b** and **12d**, but absent or much less frequent in the less active analogs. Moreover, **12c** was unique in exhibiting hydrogen bonding with Glu197 and Asn68, interactions not observed in weaker derivatives, indicating that these polar contacts are responsible for **12c** superior binding affinity. Also, Pro285 contributed to the stabilization of binding for the potent compounds but showed little to no involvement in interactions with the less active compounds. Whereas π–π stacking with Trp82 and Tyr332 was observed in both weak and potent variants, its contribution appears most significant when combined with other interactions, especially hydrogen bonding. Altogether, hydrogen bonding with Gly197, Glu197, Asn68, Pro285, and π–π stacking with Trp82 seems favorable.

The top-ranked pose of compound **12c** as a BChE inhibitor within the binding site is illustrated in Fig. 5.

The top-ranked pose of compound **12c** as an AChE inhibitor within the binding site is illustrated in Fig. 6.

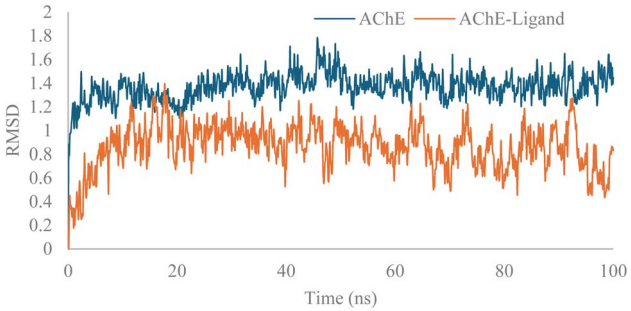


Fig. 11 RMSD of BChE *vs.* **12c**-AChE.

### 2.6 Molecular dynamics simulations

To examine the binding stability, MD simulations were run for the **12c**-BChE complex. As shown in Fig. 7, the inhibited BChE exhibited slight structural variation and reached equilibrium after approximately 35 ns. The average RMSD value for the compound binding stability within the enzyme's active site was 1.0 Å. In comparison, BChE alone achieved stability after 33 ns with an average RMSD of 1.4 Å. These findings confirm that the overall folding of the ternary complex remained essentially stable throughout the simulation.

Following this trend, the ligand exhibited minimal fluctuations within the enzyme's binding site, as indicated by RMSF values. All atoms showed RMSF values below 2 Å, except for number 48, which displayed a slightly higher RMSF of 2.3 Å. These data confirm the stability of the ligand within the active site of BChE (Fig. 8).

Based on the outcomes of molecular docking and MD simulation, it was determined that all **12c** moieties participated in interactions with various binding pockets of the enzyme. Analyzing the interactions between the ligand and amino acid residues in the protein's active site is a crucial part of assessing the stability of the protein–ligand complex. The analysis of the full MD simulation run (0–100 ns) showed that the complex formed multiple stable interactions during the simulation, the amide linker attached to the 2-fluorophenyl formed hydrogen

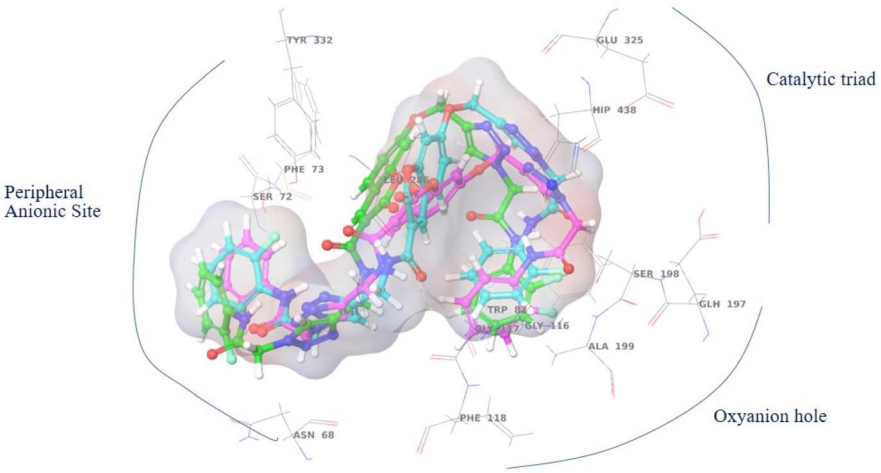


Fig. 10 The conformation of **12c** over different time trajectories during MD simulation.

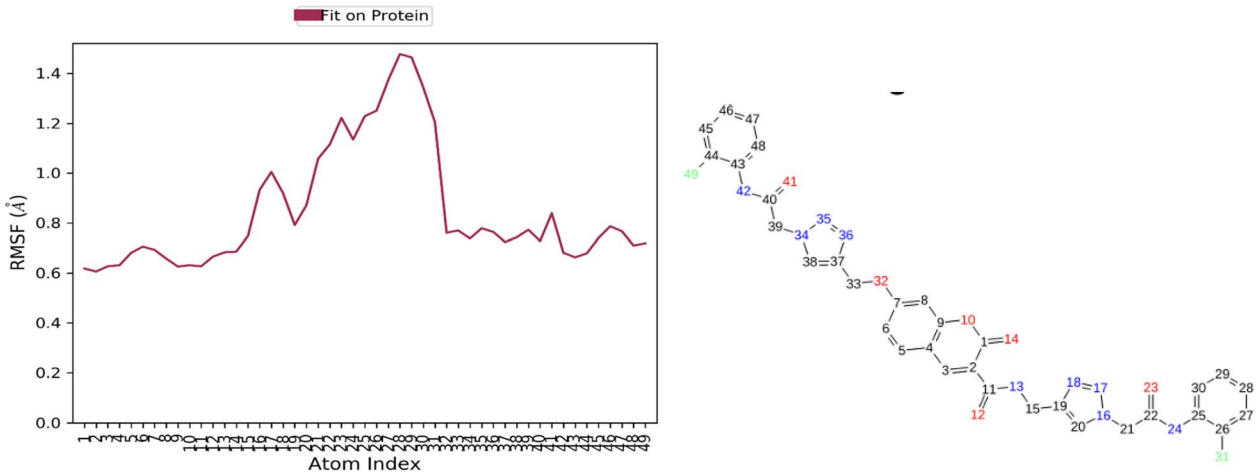


Fig. 12 RMSD of **12c** in the active site of AChE.

bond with Asp70 of the peripheral anionic site which facilitated interactions with the entrance of the enzyme's binding site, and the triazole moiety attached to this linker interacted with Ser287.

Also, the amide linker attached to the chromenone core formed several hydrogen-bond interactions with Pro285, mediated by a water molecule and residues in the oxanion hole region, such as Gly117, Gln119, and Thr120. The MD simulation demonstrates that water molecules mediate the stabilization of the complex, as underscored by these water-bridged interactions (Fig. 9).

Additionally, the chromenone core established two hydrogen bonds, both mediated by water molecules: one with Gly116 (the oxanion hole area) and another with His438 (a member of the catalytic triad). Two hydrogen bonds involving the amide linker connected to the terminal 2-fluorophenyl group were established with Glu197 and Ser198 (catalytic triad). The current docking study repeatedly found this pattern of interaction. The methoxy triazole linker contributed to binding stability by participating in π–π stacking interactions with Trp430.

The compound's 3D interaction behavior within the BChE binding pocket was assessed at the start, middle, and end of the simulation to verify its stability and occupation over time. The results showed that the compound adopted an S-shaped conformation during the MD run, confirming that various moieties of the molecule successfully occupied distinct pockets of the enzyme during the simulation (Fig. 10). Based on the outcomes of molecular docking and MD simulation, it was determined that all **12c** moieties participated in interactions with various binding pockets of the enzyme.

Molecular dynamics simulation of **12c** in the AChE active site was also performed, and the RMSD of the **12c**-AChE *vs.* AChE complexes are shown in Fig. 11. The apo enzyme and the ligand-bound complex displayed structural stability within the 100 ns simulation. The apo AChE had an average RMSD of

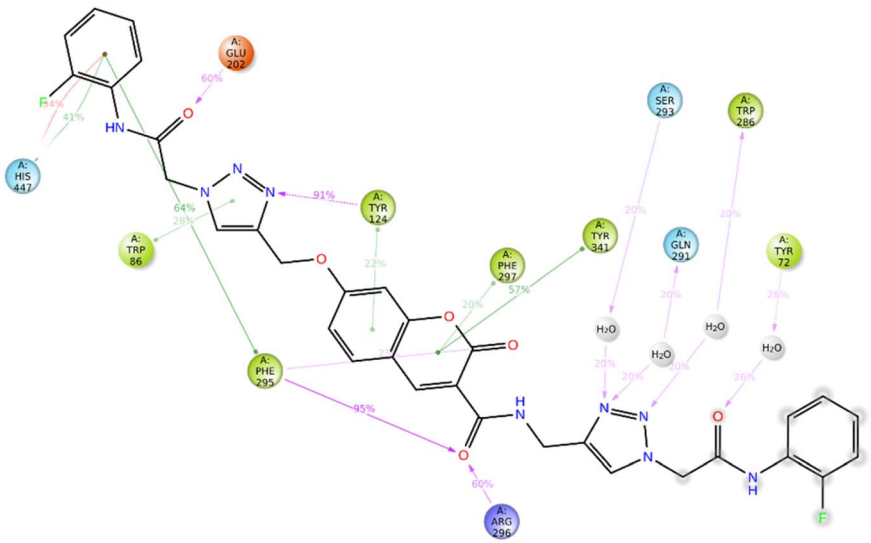


Fig. 13 A schematic of detailed **12c** atom interactions with the protein residues. Interactions that occur more than 20.0% of the simulation time in the selected trajectory.

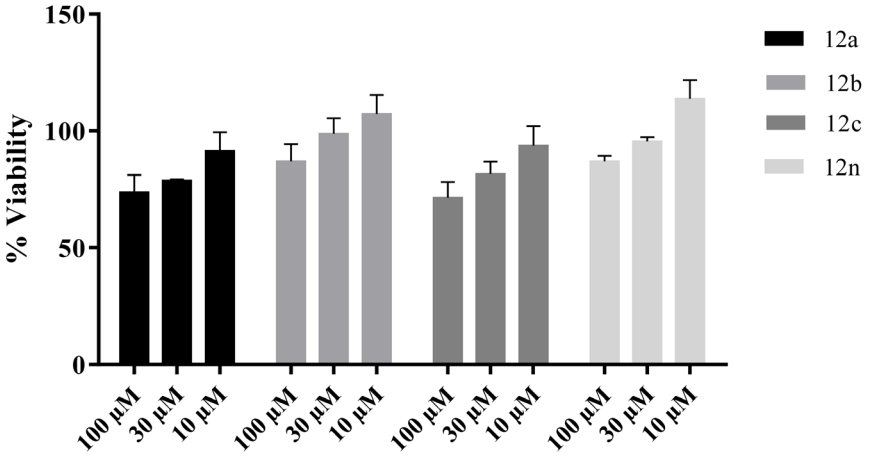


Fig. 14 Cytotoxicity study of **12a**, **12b**, **12c** and **12r** against the SH-SY5Y.

Table 4 Physicochemical properties of the synthesized compounds **12a**, **12b**, **12c** and **12n**

| Compound | $M_W$ (Da) | log *P* | HBA | HBD | tPSA (Å$^2$) | RB |
|---|---|---|---|---|---|---|
| **12a** | 633.625 | 2.7624 | 12 | 3 | 265.701 | 12 |
| **12b** | 661.680 | 3.3792 | 12 | 3 | 278.431 | 12 |
| **12c** | 669.605 | 3.0406 | 12 | 3 | 274.032 | 12 |
| **12n** | 689.733 | 3.9960 | 12 | 3 | 291.161 | 12 |

approximately 1.5 Å, whereas the **12c**-AChE complex showed a lower RMSD value of approximately 0.9 Å. This reduction of RMSD upon ligand binding suggests that compound **12c** facilitates the stabilization of the structure of AChE during the simulation (Fig. 11).

Additionally, all atoms of the ligand exhibited RMSF values below 2 Å, indicating minimal atomic fluctuations during the simulation. These results confirm the structural stability of the ligand within the active site of AChE (Fig. 12).

**12c** binding interactions with AChE were also investigated. One of the 2-fluorophenyl groups exhibited both π-cation and π–π stacking interactions with His447, a crucial residue of the catalytic triad. The amide linker among the 2-fluorophenyl ring formed hydrogen bonds with Tyr72 (*via* a water molecule) and Glu202. The 1,2,4-triazole ring was involved in direct hydrogen bonding with Tyr124, π–π stacking with Trp86, and three water-assisted hydrogen bonds with Ser293, Glu291, and Trp286. The chromenone core was also involved in some stabilizing interactions like π–π stacking with Tyr124, Phe297, and Tyr341, and one hydrogen bond with Phe295 (Fig. 13).

### 2.7 Cell cytotoxicity

The most active derivatives were tested for cytotoxicity in the SH-SY5Y neuroblastoma cell line (Pasteur Institute of Iran (https://en.pasteur.ac.ir/)) to estimate their neurotoxicity. Cell viability was assessed 72 h after treatment, and the results are summarized in Fig. 14. The data indicate that all compounds showed no significant cytotoxicity at 10 μM and maintained >80% cell viability at 30 μM. At 10 μM, all derivatives showed cell viability greater than 70%. Given the $IC_{50}$ value of compound **12c**, this analogue can be considered relatively safe under the tested conditions.

### 2.8 Prediction of pharmacokinetic properties

These physicochemical attributes are essential for developing effective treatments for neurological disorders.[23] As summarized in Table 4, all selected compounds exhibit molecular weights ranging from 633.62 to 689.73 Da. The number of rotatable bonds is consistent across the series (RB = 12), indicating a comparable degree of molecular flexibility. The calculated topological polar surface area (tPSA) values range from 265.70 to 291.16 Å$^2$, reflecting the relatively polar nature of these structures. All compounds contain 12 hydrogen-bond acceptors and 3 hydrogen-bond donors, suggesting similar hydrogen-bonding capacities across the series. The calculated Log *P* values (2.76–3.99) indicate moderate lipophilicity, remaining within commonly accepted limits for oral drug candidates.

ADME predictions (Table 5) revealed moderate to high predicted intestinal absorption (67.60–72.32%), suggesting acceptable gastrointestinal uptake. All compounds were

Table 5 ADMEa prediction of the synthesized compounds **12a**, **12b**, **12c** and **12n**

| Compound | VDss (human) | Intestinal absorption (%) | P-gp substrate | CYP3A4 inhibitor | CYP2C19 inhibitor | CYP1A2 inhibitor | CYP2D6 substrate | CYP3A4 substrate |
|---|---|---|---|---|---|---|---|---|
| **12a** | −0.727 | 71.38 | Yes | Yes | No | No | No | Yes |
| **12b** | −0.694 | 72.316 | Yes | Yes | No | No | No | Yes |
| **12c** | −0.821 | 67.605 | Yes | Yes | No | No | No | Yes |
| **12n** | −0.66 | 73.253 | Yes | Yes | No | No | No | Yes |

predicted to be P-glycoprotein (P-gp) substrates and CYP3A4 substrates, and to act as CYP3A4 inhibitors, indicating potential susceptibility to efflux transport and drug–drug interactions. None of the compounds were predicted to inhibit CYP2C19 or CYP1A2, and none were predicted to act as CYP2D6 substrates.

# 3. Conclusion

In this study, a series of triazole hybrids (**12a–s**) were successfully synthesized and their inhibitory activities against BChE and AChE enzymes were evaluated. The results showed that structural modifications, particularly the positions of substituents, significantly affect biological activity. In terms of BChE inhibition, compounds with 2-position substituents, particularly 2-fluorophenyl (compound **12c**, $IC_{50} = 4.37 \pm 0.91$ μM), generally increased potency, while compounds with 2-position substituents showed the second-highest activity. As demonstrated by compound **12n** (2,4-dimethylphenyl; $IC_{50} = 6.65 \pm 1.31$ μM), disubstitution at the 2,4-positions enhanced binding affinity, highlighting the advantageous effects of dual substitutions. Overall, the study showed that although steric hindrance and excessive bulk reduce activity, small electron-withdrawing groups, especially fluorine are quite effective at boosting enzyme inhibition. Through docking assessments, compound **12c** showed a substantial binding affinity to both AChE and BChE. The stability of the **12c**-enzyme complexes was validated by MD over 100 ns, which showed persistent hydrogen bonding and low RMSD values.

These findings provide valuable insights into the structure–activity relationships of triazole hybrids and establish a foundation for further optimization and development of potent cholinesterase inhibitors for therapeutic applications in Alzheimer's disease.

# 4. Method and materials

## 4.1 Chemistry

**4.1.1 2-oxo-7-((1-(2-oxo-2-(Phenylamino)ethyl)-1*H*-1,2,3-triazol-4-yl)methoxy)-*N*-((1-(2-oxo-2-(phenylamino)ethyl)-1*H*-1,2,3-triazol-4-yl)methyl)-2*H*-chromene-3-carboxamide (12a).** Brown solid; yield: 67%; MP = 212–214 °C; IR (KBr, $\nu_{max}$) 3310 (NH), 3016 (CH aromatic), 2945 (CH aliphatic), 1662 (C=O) $cm^{-1}$; $^1$H NMR (500 MHz, DMSO-$d_6$) $\delta$ 10.48 (s, 1H), 10.44 (s, 1H), 9.10 (t, $J$ = 4.8 Hz, 1H), 8.87 (s, 1H), 8.33 (s, 1H), 8.05 (s, 1H), 7.93 (d, $J$ = 8.7 Hz, 1H), 7.62–7.50 (m, 4H), 7.37–7.26 (m, 5H), 7.13 (d, $J$ = 8.4 Hz, 1H), 7.10–7.04 (m, 2H), 5.37–5.34 (m, 4H), 5.31 (s, 2H), 4.62 (d, $J$ = 4.5 Hz, 2H): $^{13}$C NMR (126 MHz, DMSO-$d_6$) $\delta$ 164.16, 164.08, 163.14, 161.39, 160.78, 156.07, 147.94, 138.37, 138.34, 131.62, 128.85, 126.68, 124.59, 123.76, 123.73, 119.23, 114.84, 114.08, 112.33, 101.15, 61.90, 52.23, 52.19, 34.80; anal. calcd; $C_{32}H_{27}N_9O_6$; C, 60.66; H, 4.30; N, 19.90; found; C, 60.82; H, 4.48; N, 20.08.

**4.1.2 2-oxo-7-((1-(2-oxo-2-(*o*-Tolylamino)ethyl)-1*H*-1,2,3-triazol-4-yl)methoxy)-*N*-((1-(2-oxo-2-(*o*-tolylamino)ethyl)-1*H*-1,2,3-triazol-4-yl)methyl)-2*H*-chromene-3-carboxamide (12b).** Brown solid; yield: 78%; MP = 222–225 °C; IR (KBr, $\nu_{max}$) 3315 (NH), 3025 (CH aromatic), 2850 (CH aliphatic), 1663 (C=O) $cm^{-1}$; $^1$H NMR (500 MHz, DMSO-$d_6$) $\delta$ 9.80 (s, 1H), 9.76 (s, 1H), 9.10 (t, $J$ = 5.5 Hz, 1H), 8.87 (s, 1H), 8.33 (s, 1H), 8.05 (s, 1H), 7.93 (d, $J$ = 8.8 Hz, 1H), 7.41 (d, $J$ = 7.8 Hz, 2H), 7.31 (d, $J$ = 1.9 Hz, 1H), 7.22 (d, $J$ = 7.2 Hz, 2H), 7.18–7.12 (m, 3H), 7.12–7.07 (m, 3H), 5.41 (s, 2H), 5.36 (s, 2H), 5.34 (s, 2H), 4.61 (d, $J$ = 5.2 Hz, 2H), 2.23–2.21 (m, 6H): $^{13}$C NMR (126 MHz, DMSO-$d_6$) $\delta$ 164.86, 164.78, 163.64, 161.88, 161.28, 156.58, 148.45, 144.61, 141.98, 135.99, 135.96, 132.12, 132.06, 130.90, 127.17, 126.52, 126.04, 126.01, 125.20, 125.03, 115.34, 114.59, 112.83, 101.64, 62.39, 52.45, 52.41, 35.30, 18.23; anal. calcd; $C_{34}H_{31}N_9O_6$; C, 61.72; H, 4.72; N, 19.05; found; C, 61.91; H, 4.87; N, 19.28.

**4.1.3 7-((1-(2-((2-Fluorophenyl)amino)-2-oxoethyl)-1*H*-1,2,3-triazol-4-yl)methoxy)-*N*-((1-(2-((2-fluorophenyl)amino)-2-oxoethyl)-1*H*-1,2,3-triazol-4-yl)methyl)-2-oxo-2*H*-chromene-3-carboxamide (12c).** Brown solid; yield: 65%; MP = 230–232 °C; IR (KBr, $\nu_{max}$) 3350 (NH), 3040 (C–H aromatic), 2960 (CH aliphatic), 1667 (C=O) $cm^{-1}$; $^1$H NMR (500 MHz, DMSO-$d_6$) $\delta$ 10.33 (s, 1H), 10.29 (s, 1H), 9.10 (t, $J$ = 5.2 Hz, 1H), 8.88 (s, 1H), 8.80 (s, 1H), 8.67 (d, $J$ = 14.2 Hz, 1H), 8.32 (s, 1H), 8.04 (s, 1H), 7.94 (d, $J$ = 8.7 Hz, 1H), 7.92–7.86 (m, 2H), 7.33–7.24 (m, 2H), 7.22–7.08 (m, 4H), 5.45 (s, 2H), 5.40 (s, 2H), 5.35 (s, 2H), 4.61 (d, $J$ = 5.1 Hz, 2H): $^{13}$C NMR (126 MHz, DMSO-$d_6$) $\delta$ 164.84, 164.80, 163.18, 161.61., 160.90, 157.57, 156.18, 153.54 (d, $J$ = 246.0 Hz), 148.09, 141.73, 135.94, 131.74, 130.76, 126.85, 125.77, 125.55, 124.54, 123.81, 120.37, 115.75, 115.60, 114.20, 11.85, 101.59, 101.21, 61.97, 52.07, 52.04, 34.90; anal. calcd; $C_{32}H_{25}F_2N_9O_6$; C, 57.40; H, 3.76; N, 18.83; found; C, 57.56; H, 3.91; N, 19.02. The purity of the compound was checked using HPLC (98.2% purity).

**4.1.4 7-((1-(2-((2-Chlorophenyl)amino)-2-oxoethyl)-1*H*-1,2,3-triazol-4-yl)methoxy)-*N*-((1-(2-((2-chlorophenyl)amino)-2-oxoethyl)-1*H*-1,2,3-triazol-4-yl)methyl)-2-oxo-2*H*-chromene-3-carboxamide (12d).** Cream solid; yield: 61%; MP = 239–241 °C; IR (KBr, $\nu_{max}$) 3330 (NH), 3040 (CH aromatic), 2960 (CH aliphatic), 1662 (C=O) $cm^{-1}$; $^1$H NMR (500 MHz, DMSO-$d_6$) $\delta$ 10.09 (s, 1H), 10.04 (s, 1H), 9.10 (t, $J$ = 4.8 Hz, 1H), 8.87 (s, 1H), 8.33 (s, 1H), 8.05 (s, 1H), 7.93 (d, $J$ = 8.7 Hz, 1H), 7.72 (d, $J$ = 8.1 Hz, 2H), 7.51 (d, $J$ = 9.0 Hz, 2H), 7.37–7.29 (m, 3H), 7.27–7.17 (m, 2H), 7.12 (d, $J$ = 10.8 Hz, 1H), 5.47 (s, 2H), 5.41 (s, 2H), 5.35 (s, 2H), 4.61 (d, $J$ = 4.6 Hz, 2H): $^{13}$C NMR (126 MHz, DMSO-$d_6$) $\delta$ 165.01, 164.93, 163.23, 161.50, 160.90, 148.09, 134.23, 134.21, 131.74, 129.69, 127.63, 126.85, 126.38, 126.11, 125.78, 124.78, 114.91, 114.21, 112.43, 101.23, 61.96, 52.07, 52.01, 34.92; anal. calcd; $C_{32}H_{25}C_{12}N_9O_6$; C, 54.71; H, 3.59; N, 17.94; found; C, 54.93; H, 3.76; N, 18.14.

**4.1.5 2-oxo-7-((1-(2-oxo-2-(*m*-Tolylamino)ethyl)-1*H*-1,2,3-triazol-4-yl)methoxy)-*N*-((1-(2-oxo-2-(*m*-tolylamino)ethyl)-1*H*-1,2,3-triazol-4-yl)methyl)-2*H*-chromene-3-carboxamide (12e).** Brown solid; yield: 71%; MP = 251–253 °C; IR (KBr, $\nu_{max}$) 3325 (NH), 3049 (C–H aromatic), 2963 (CH aliphatic), 1665 (C=O) $cm^{-1}$; $^1$H NMR (500 MHz, DMSO-$d_6$) $\delta$ 10.67–10.27 (m, 2H), 9.11 (s, 1H), 8.88 (s, 1H), 8.33 (s, 1H), 8.04 (s, 1H), 7.93 (t, $J$ = 5.8 Hz, 1H), 7.40 (s, 1H), 7.38–7.33 (m, 2H), 7.31 (s, 1H), 7.27–7.16 (m, 3H), 7.13 (d, $J$ = 9.0 Hz, 1H), 6.99–6.75 (m, 2H), 5.35 (m, 4H), 5.30 (s, 2H), 4.61 (d, $J$ = 5.7 Hz, 2H), 2.41–2.11 (m, 6H); $^{13}$C NMR (126 MHz, DMSO-$d_6$) $\delta$ 164.15, 164.11, 164.06, 163.15, 161.42, 160.84, 156.11, 148.03, 141.45, 138.33, 138.13, 131.67, 128.74, 126.79,

124.49, 124.46, 119.75, 116.39, 114.81, 114.12, 112.35, 101.12, 61.88, 52.26, 52.20, 34.82, 21.15; anal. calcd; $C_{34}H_{31}N_9O_6$; C, 61.72; H, 4.72; N, 19.05; found; C, 61.90; H, 4.91; N, 19.25.

**4.1.6 7-((1-(2-((3-Chlorophenyl)amino)-2-oxoethyl)-1*H*-1,2,3-triazol-4-yl)methoxy)-*N*-((1-(2-((3-chlorophenyl)amino)-2-oxoethyl)-1*H*-1,2,3-triazol-4-yl)methyl)-2-oxo-2*H*-chromene-3-carboxamide (12f).** Cream solid; yield: 63%; MP = 235–237 °C; IR (KBr, $\nu_{max}$) 3320 (NH), 3040 (CH aromatic), 2950 (CH aliphatic), 1665 (C=O) $cm^{-1}$, $^1H$ NMR (500 MHz, DMSO-$d_6$) $\delta$ 10.09 (s, 1H), 10.04 (s, 1H), 9.10 (t, $J$ = 5.1 Hz, 1H), 8.87 (s, 1H), 8.33 (s, 1H), 8.05 (s, 1H), 7.93 (d, $J$ = 8.7 Hz, 1H), 7.85 (d, $J$ = 8.5 Hz, 1H), 7.73 (d, $J$ = 7.7 Hz, 2H), 7.55–7.47 (m, 2H), 7.38–7.29 (m, 2H), 7.27–7.17 (m, 2H), 7.13 (d, $J$ = 8.8 Hz, 1H), 5.47 (s, 2H), 5.42 (s, 2H), 5.35 (s, 2H), 4.61 (d, $J$ = 4.7 Hz, 2H): $^{13}C$ NMR (126 MHz, DMSO-$d_6$) $\delta$ 165.00, 164.93, 163.23, 161.51, 160.90, 156.19, 148.09, 142.07, 141.64, 136.03, 134.24, 134.22, 131.75, 130.74, 129.71, 129.69, 127.64, 126.83, 126.80, 126.41, 126.30, 125.97, 125.93, 124.81, 124.72, 114.91, 114.21, 112.44, 111.81, 101.24, 61.96, 59.83, 52.06, 52.02, 34.92, 20.83, 14.16; anal. calcd; $C_{32}H_{25}C_{12}N_9O_6$; C, 54.71; H, 3.59; N, 17.94; found; C, 54.92; H, 3.77; N, 18.15.

**4.1.7 2-oxo-7-((1-(2-oxo-2-(*p*-Tolylamino)ethyl)-1*H*-1,2,3-triazol-4-yl)methoxy)-*N*-((1-(2-oxo-2-(*p*-tolylamino)ethyl)-1*H*-1,2,3-triazol-4-yl)methyl)-2*H*-chromene-3-carboxamide (12g).** Brown solid; yield: 79%; MP = 220–223 °C; IR (KBr, $\nu_{max}$) 3330 (NH), 3035 (CH aromatic), 2850 (CH aliphatic), 1666 (C=O) $cm^{-1}$, $^1H$ NMR (500 MHz, DMSO-$d_6$) $\delta$ 10.35 (s, 1H), 10.32 (s, 1H), 9.08 (t, $J$ = 4.9 Hz, 1H), 8.87 (s, 1H), 8.31 (s, 1H), 8.03 (s, 1H), 7.93 (d, $J$ = 8.7 Hz, 1H), 7.48–7.42 (m, 4H), 7.30 (s, 1H), 7.16–7.05 (m, 5H), 5.35 (s, 2H), 5.33 (s, 2H), 5.27 (s, 2H), 4.61 (d, $J$ = 5.1 Hz, 2H), 2.24 (s, 6H): $^{13}C$ NMR (126 MHz, DMSO-$d_6$) $\delta$ 164.39, 164.30, 163.58, 161.87, 161.27, 156.58, 148.51, 146.10, 141.96, 136.36, 136.34, 133.25, 132.13, 132.11, 129.72, 129.71, 129.70, 127.21, 127.18, 125.07, 119.76, 115.29, 114.54, 112.83, 101.64, 62.30, 52.71, 52.70, 35.32, 20.87; anal. calcd; $C_{34}H_{31}N_9O_6$; C, 61.72; H, 4.72; N, 19.05; found; C, 62.12; H, 5.15; N, 19.41. HRMS (TOF MS E+) $m/z$ calcd for $C_{34}H_{31}N_9O_6Na$ $[M + Na]^+$ 684.6697; found 684.3505.

**4.1.8 7-((1-(2-((4-Ethylphenyl)amino)-2-oxoethyl)-1*H*-1,2,3-triazol-4-yl)methoxy)-*N*-((1-(2-((4-ethylphenyl)amino)-2-oxoethyl)-1*H*-1,2,3-triazol-4-yl)methyl)-2-oxo-2*H*-chromene-3-carboxamide (12h).** Cream solid; yield: 68%; MP = 212–214 °C; IR (KBr, $\nu_{max}$) 3230 (NH), 3025 (CH aromatic), 2945 (CH aliphatic), 1663 (C=O) $cm^{-1}$, $^1H$ NMR (500 MHz, DMSO-$d_6$) $\delta$ 10.40 (s, 1H), 10.37 (s, 1H), 9.10 (t, $J$ = 5.0 Hz, 1H), 8.88 (s, 1H), 8.32 (s, 1H), 8.04 (s, 1H), 7.93 (d, $J$ = 8.8 Hz, 1H), 7.47 (d, $J$ = 8.1 Hz, 4H), 7.31 (s, 1H), 7.20–7.09 (m, 5H), 5.36–5.33 (m, 4H), 5.28 (s, 2H), 4.61 (d, $J$ = 5.2 Hz, 2H), 2.54 (q, $J$ = 7.2 Hz, 4H), 1.14 (t, $J$ = 7.4 Hz, 6H); $^{13}C$ NMR (126 MHz, DMSO-$d_6$) $\delta$ 164.05, 163.97, 163.26, 161.52, 160.93, 156.20, 148.10, 141.56, 139.29, 136.18, 131.75, 128.17, 126.86, 119.41, 114.91, 114.22, 112.45, 101.24, 61.99, 52.32, 52.27, 34.93, 27.66, 15.67; anal. calcd; $C_{36}H_{35}N_9O_6$; C, 62.69; H, 5.12; N, 18.28; found; C, 62.85; H, 5.30; N, 18.44.

**4.1.9 7-((1-(2-((4-Methoxyphenyl)amino)-2-oxoethyl)-1*H*-1,2,3-triazol-4-yl)methoxy)-*N*-((1-(2-((4-methoxyphenyl)amino)-2-oxoethyl)-1*H*-1,2,3-triazol-4-yl)methyl)-2-oxo-2*H*-chromene-3-carboxamide (12i).** Brown solid; yield: 77%; MP = 253–255 °C; IR (KBr, $\nu_{max}$) 3328 (NH), 3042 (C–H aromatic), 2964 (CH aliphatic), 1663 (C=O) $cm^{-1}$; 1H NMR (400 MHz, DMSO-$d_6$) $\delta$ 10.57–10.20 (m, 2H), 9.13 (t, $J$ = 5.8 Hz, 1H), 8.90 (s, 1H), 8.35 (s, 1H), 8.06 (s, 1H), 7.96 (d, $J$ = 8.6 Hz, 1H), 7.50 (d, $J$ = 8.6 Hz, 4H), 7.34 (d, $J$ = 2.4 Hz, 1H), 7.15 (dd, $J$ = 8.7, 2.4 Hz, 1H), 6.97–6.85 (m, 4H), 5.40–5.33 (m, 4H), 5.29 (s, 2H), 4.63 (d, $J$ = 5.6 Hz, 2H), 3.72 (s, 6H); $^{13}C$ NMR (101 MHz, DMSO-$d_6$) $\delta$ 164.16, 164.08, 163.62, 163.59, 162.11, 161.89, 161.31, 156.59, 155.96, 148.51, 132.16, 131.98, 131.95, 127.28, 121.21, 121.20, 114.61, 114.47, 114.42, 55.61, 52.59, 52.58, 42.99; anal. calcd; $C_{34}H_{31}N_9O_8$; C, 58.87; H, 4.50; N, 18.17; found; C, 59.03; H, 4.68; N, 18.37.

**4.1.10 7-((1-(2-((4-Fluorophenyl)amino)-2-oxoethyl)-1*H*-1,2,3-triazol-4-yl)methoxy)-*N*-((1-(2-((4-fluorophenyl)amino)-2-oxoethyl)-1*H*-1,2,3-triazol-4-yl)methyl)-2-oxo-2*H*-chromene-3-carboxamide (12j).** Brown solid; yield: 74%; MP = 239–241 °C; IR (KBr, $\nu_{max}$) 3350 (NH), 3025 (C–H aromatic), 2980 (CH aliphatic), 1669 (C=O) $cm^{-1}$; $^1H$ NMR (500 MHz, DMSO-$d_6$) $\delta$ 10.56 (s, 1H), 10.52 (s, 1H), 9.10 (t, $J$ = 4.7 Hz, 1H), 8.87 (s, 1H), 8.33 (s, 1H), 8.05 (s, 1H), 7.93 (d, $J$ = 8.7 Hz, 1H), 7.68–7.51 (m, 4H), 7.31 (s, 1H), 7.24–7.12 (m, 5H), 5.38–5.33 (m, 4H), 5.30 (s, 2H), 4.61 (d, $J$ = 4.7 Hz, 2H): $^{13}C$ NMR (126 MHz, DMSO-$d_6$) $\delta$ 164.25, 164.17, 163.23, 161.51, 160.91, 158.34 (d, $J$ = 238.5 Hz), 156.17, 148.08, 141.62, 134.85, 134.84, 134.82, 131.72, 126.84, 124.74, 121.14 (d, $J$ = 7.8 Hz), 115.56 (d, $J$ = 22.3 Hz), 114.88, 114.19, 112.43, 101.22, 61.98, 52.27, 52.23, 34.92; $^{19}F$ NMR (471 MHz, DMSO-$d_6$) $\delta$ −118.65 (dtt, $J$ = 21.3, 8.7, 4.8 Hz); anal. calcd; $C_{32}H_{25}F_2N_9O_6$; C, 57.40; H, 3.76; N, 18.83; found; C, 57.62; H, 3.91; N, 18.98.

**4.1.11 7-((1-(2-((4-Chlorophenyl)amino)-2-oxoethyl)-1*H*-1,2,3-triazol-4-yl)methoxy)-*N*-((1-(2-((4-chlorophenyl)amino)-2-oxoethyl)-1*H*-1,2,3-triazol-4-yl)methyl)-2-oxo-2*H*-chromene-3-carboxamide (12k).** Brown solid; yield: 68%; MP = 240–242 °C; IR (KBr, $\nu_{max}$) 3320 (NH), 3030 (CH aromatic), 2940 (CH aliphatic),1662 (C=O) $cm^{-1}$; $^1H$ NMR (500 MHz, DMSO-$d_6$) $\delta$ 10.62 (s, 1H, NH), 10.59 (s, 1H, NH), 9.10 (t, $J$ = 5.5 Hz, 1H, H13), 8.88 (s, 1H, triazole), 8.33 (s, 1H, triazole), 8.04 (s, 1H, H6), 7.94 (d, $J$ = 8.8 Hz, 1H, H6), 7.59 (d, $J$ = 8.1 Hz, 4H), 7.40–7.36 (m, 4H), 7.31 (d, $J$ = 2.0 Hz, 1H, H3), 7.13 (dd, $J$ = 8.7, 2.2 Hz, 1H, H1), 5.37 (s, 2H, $CH_2$), 5.35 (s, 2H, $CH_2$), 5.31 (s, 2H, $CH_2$), 4.61 (d, $J$ = 5.3 Hz, 2H, H15): $^{13}C$ NMR (126 MHz, DMSO-$d_6$) $\delta$ 164.90 (C39 or C22), 164.82 (C39 or C22), 163.65, 161.90, 161.30, 156.44, 148.48, 137.84, 137.81, 132.14, 129.31, 129.30, 127.90, 127.87, 127.20, 125.11, 121.32, 115.35, 114.61, 112.85, 101.66 (C3), 62.39 (C32), 52.72 ($CH_2$), 52.66 ($CH_2$), 35.45 (C15); anal. calcd; $C_{23}H_{21}N_3O_4$; C, 54.71; H, 3.59; N, 17.94; found; C, 54.93; H, 3.71; N, 18.09.

**4.1.12 7-((1-(2-((4-Bromophenyl)amino)-2-oxoethyl)-1*H*-1,2,3-triazol-4-yl)methoxy)-*N*-((1-(2-((4-bromophenyl)amino)-2-oxoethyl)-1*H*-1,2,3-triazol-4-yl)methyl)-2-oxo-2*H*-chromene-3-carboxamide (12l).** Brown solid; yield: 72%; MP = 242–244 °C; IR (KBr, $\nu_{max}$) 3330 (NH), 3010 (CH aromatic), 2860 (CH aliphatic), 1659 (C=O) $cm^{-1}$; $^1H$ NMR (500 MHz, DMSO-$d_6$) $\delta$ 10.62 (s, 1H), 10.59 (s, 1H), 9.09 (t, $J$ = 5.6 Hz, 1H), 8.88 (s, 1H), 8.32 (s, 1H), 8.04 (s, 1H), 7.94 (d, $J$ = 8.8 Hz, 1H), 7.55–7.54 (m,

1H), 7.54–7.53 (m, 3H), 7.52–7.50 (m, 3H), 7.50–7.49 (m, 1H), 7.31 (d, $J$ = 2.2 Hz, 1H), 7.13 (dd, $J$ = 8.7, 2.3 Hz, 1H), 5.36 (s, 2H), 5.35 (s, 2H), 5.31 (s, 2H), 4.61 (d, $J$ = 5.4 Hz, 2H): $^{13}$C NMR (126 MHz, DMSO-$d_6$) $\delta$ 164.90, 164.82, 163.63, 161.88, 161.28, 156.58, 148.46, 142.01, 138.24, 138.21, 132.22, 132.20, 127.19, 121.66, 115.90, 115.87, 115.34, 114.59, 112.83, 101.65, 62.38, 52.72, 52.67, 35.29; anal. calcd; $C_{32}H_{25}Br_2N_9O_6$; C, 48.57; H, 3.18; N, 15.93; found; C, 48.82; H, 3.36; N, 16.12.

**4.1.13 2-oxo-7-((1-(2-oxo-2-((4-(Trifluoromethyl)phenyl) amino)ethyl)-1*H*-1,2,3-triazol-4-yl)methoxy)-*N*-((1-(2-oxo-2-((4-(trifluoromethyl)phenyl)amino)ethyl)-1*H*-1,2,3-triazol-4-yl) methyl)-2*H*-chromene-3-carboxamide (12m).** Brown solid; yield: 75%; MP = 286–288 °C; IR (KBr, $\nu_{max}$) 3325 (NH), 3053 (C–H aromatic), 2961 (CH aliphatic), 1663 (C=O) cm$^{-1}$; $^1$H NMR (500 MHz, DMSO-$d_6$) $\delta$ 11.13–10.51 (m, 2H), 9.11 (t, $J$ = 5.7 Hz, 1H), 8.88 (s, 1H), 8.35 (s, 1H), 8.07 (s, 1H), 7.93 (d, $J$ = 8.7 Hz, 1H), 7.78 (d, $J$ = 8.3 Hz, 4H), 7.74–7.65 (m, 4H), 7.31 (d, $J$ = 2.4 Hz, 1H), 7.12 (dd, $J$ = 8.8, 2.4 Hz, 1H), 5.43 (s, 2H), 5.40–5.30 (m, 4H), 4.62 (d, $J$ = 5.6 Hz, 2H); $^{13}$C NMR (126 MHz, DMSO-$d_6$) $\delta$ 165.41, 165.33, 163.55, 161.82, 161.24, 156.51, 148.43, 142.36 (d, $J$ = 3.2 Hz), 141.96, 132.07, 127.91, 127.22 (d, $J$ = 3.3 Hz), 126.82–126.52 (m), 125.75, 125.11, 124.31 (d, $J$ = 4.3 Hz), 124.05 (d, $J$ = 4.4 Hz), 123.60, 119.57, 115.21, 114.53, 112.76, 101.53, 62.28, 52.69, 52.63, 35.23; anal. calcd; $C_{34}H_{25}F_6N_9O_6$; C, 53.06; H, 3.27; N, 16.38; found; C, 53.21; H, 3.42; N, 16.55.

**4.1.14 7-((1-(2-((2,4-Dimethylphenyl)amino)-2-oxoethyl)-1*H*-1,2,3-triazol-4-yl)methoxy)-*N*-((1-(2-((2,4-dimethylphenyl) amino)-2-oxoethyl)-1*H*-1,2,3-triazol-4-yl)methyl)-2-oxo-2*H*-chromene-3-carboxamide (12n).** Brown solid; yield: 74%; MP = 232–235 °C; IR (KBr, $\nu_{max}$) 3325 (NH), 3035 (CH aromatic), 2840 (CH aliphatic), 1666 (C=O) cm$^{-1}$, $^1$H NMR (500 MHz, DMSO-$d_6$) $\delta$ 9.74 (s, 1H), 9.69 (s, 1H), 9.10 (t, $J$ = 4.9 Hz, 1H), 8.87 (s, 1H), 8.32 (s, 1H), 8.04 (s, 1H), 7.92 (d, $J$ = 8.6 Hz, 1H), 7.30 (s, 1H), 7.26 (d, $J$ = 7.9 Hz, 2H), 7.12 (d, $J$ = 8.3 Hz, 1H), 7.04–7.00 (m, 2H), 6.99–6.93 (m, 2H), 5.38 (s, 2H), 5.36–5.31 (m, 4H), 4.61 (d, $J$ = 5.1 Hz, 2H), 2.23 (s, 6H), 2.17 (s, 6H): $^{13}$C NMR (126 MHz, DMSO-$d_6$) $\delta$ 164.42, 164.34, 163.30, 163.24, 161.49, 161.41, 160.90, 160.78, 156.22, 156.18, 148.25, 148.09, 142.04, 141.58, 134.80, 134.75, 132.99, 132.96, 131.78, 131.74, 131.63, 131.02, 114.89, 114.21, 112.41, 101.21, 80.91, 73.31, 61.97, 52.03, 51.98, 34.92, 28.75, 20.53, 17.78; anal. calcd; $C_{36}H_{35}N_9O_6$; C, 62.69; H, 5.12; N, 18.28; found; C, 62.90; H, 5.30; N, 18.42.

**4.1.15 7-((1-(2-((2,4-Dimethoxyphenyl)amino)-2-oxoethyl)-1*H*-1,2,3-triazol-4-yl)methoxy)-*N*-((1-(2-((2,4-dimethoxyphenyl) amino)-2-oxoethyl)-1*H*-1,2,3-triazol-4-yl)methyl)-2-oxo-2*H*-chromene-3-carboxamide (12o).** Brown solid; yield: 75%; MP = 239–241 °C; IR (KBr, $\nu_{max}$) 3323 (NH), 3040 (C–H aromatic), 2960 (CH aliphatic), 1667 (C=O) cm$^{-1}$; $^1$H NMR (500 MHz, DMSO-$d_6$) $\delta$ 9.62 (s, 1H), 9.57 (s, 1H), 9.09 (t, $J$ = 5.6 Hz, 1H), 8.87 (s, 1H), 8.30 (s, 1H), 8.01 (s, 1H), 7.93 (d, $J$ = 8.8 Hz, 1H), 7.69 (dd, $J$ = 8.8, 2.1 Hz, 2H), 7.31 (d, $J$ = 2.2 Hz, 1H), 7.12 (dd, $J$ = 8.7, 2.3 Hz, 1H), 6.69–6.59 (m, 2H), 6.52–6.42 (m, 2H), 5.39 (s, 2H), 5.34 (s, 4H), 4.60 (d, $J$ = 5.5 Hz, 2H), 3.83–3.82 (m, 6H), 3.74–3.71 (m, 6H): $^{13}$C NMR (126 MHz, DMSO-$d_6$) $\delta$ 164.58, 164.51, 163.65, 161.90, 161.26, 157.56, 157.54, 156.59, 151.82, 148.46, 141.98, 132.13, 127.16, 125.02, 123.85, 123.80, 120.12, 115.35, 114.60, 112.84, 104.67, 101.65, 99.42, 56.26, 55.79, 52.60, 52.55, 35.30; anal. calcd; $C_{36}H_{35}N_9O_{10}$; C, 57.37; H, 4.68; N, 16.73; found; C, 57.53; H, 4.91; N, 16.91.

**4.1.16 2-oxo-7-((1-(2-oxo-2-((3,4,5-Trimethoxyphenyl) amino)ethyl)-1*H*-1,2,3-triazol-4-yl)methoxy)-*N*-((1-(2-oxo-2-((3,4,5-trimethoxyphenyl)amino)ethyl)-1*H*-1,2,3-triazol-4-yl) methyl)-2*H*-chromene-3-carboxamide (12p).** Brown solid; yield: 73%; MP = 228–230 °C; IR (KBr, $\nu_{max}$) 3330 (NH), 3020 (CH aromatic), 2960 (CH aliphatic) 1663 (C=O) cm$^{-1}$; $^1$H NMR (500 MHz, DMSO-$d_6$) $\delta$ 10.44 (s, 1H), 10.41 (s, 1H), 9.10 (t, $J$ = 5.0 Hz, 1H), 8.87 (s, 1H), 8.32 (s, 1H), 8.03 (s, 1H), 7.94 (d, $J$ = 8.8 Hz, 1H), 7.32 (s, 1H), 7.13 (d, $J$ = 10.2 Hz, 1H), 6.94 (s, 4H), 5.35 (s, 2H), 5.33 (s, 2H), 5.28 (s, 2H), 4.61 (d, $J$ = 5.0 Hz, 2H), 3.74–3.70 (m, 12H), 3.61–3.58 (m, 6H): $^{13}$C NMR (126 MHz, DMSO-$d_6$) $\delta$ 164.15, 164.06, 163.24, 161.51, 160.92, 156.17, 152.88, 148.08, 141.64, 134.57, 134.55, 133.85, 133.82, 131.73, 126.88, 124.78, 114.86, 114.19, 112.43, 101.20, 97.06, 61.97, 60.17, 55.76, 52.34, 52.30, 34.91; anal. calcd; $C_{38}H_{39}N_9O_{12}$; C, 56.09; H, 4.83; N, 15.49; found; C, 56.26; H, 5.04; N, 15.70.

**4.1.17 7-((1-(2-(Benzylamino)-2-oxoethyl)-1*H*-1,2,3-triazol-4-yl)methoxy)-*N*-((1-(2-(benzylamino)-2-oxoethyl)-1*H*-1,2,3-triazol-4-yl)methyl)-2-oxo-2*H*-chromene-3-carboxamide (12q).** Cream solid; yield: 66%; MP = 215–217 °C; IR (KBr, $\nu_{max}$) 3280 (NH), 3010 (CH aromatic), 2945 (CH aliphatic), 1664 (C=O) cm$^{-1}$, $^1$H NMR (500 MHz, DMSO-$d_6$) $\delta$ 9.08 (t, $J$ = 5.5 Hz, 1H), 8.87 (s, 1H), 8.84 (d, $J$ = 5.4 Hz, 1H), 8.81 (t, $J$ = 5.3 Hz, 1H), 8.27 (s, 1H), 7.99 (s, 1H), 7.93 (d, $J$ = 8.8 Hz, 1H), 7.35–7.30 (m, 5H), 7.29–7.23 (m, 6H), 7.12 (dd, $J$ = 8.7, 2.3 Hz, 1H), 5.33 (s, 1H), 5.19 (s, 2H), 5.14 (s, 2H), 4.59 (d, $J$ = 5.5 Hz, 2H), 4.31 (t, $J$ = 5.4 Hz, 4H): $^{13}$C NMR (126 MHz, DMSO-$d_6$) $\delta$ 165.56, 165.48, 163.25, 161.49, 160.91, 156.18, 148.10, 141.53, 138.79, 131.74, 128.44, 127.47, 127.15, 127.01, 126.82, 126.62, 124.63, 114.89, 114.21, 112.43, 101.21, 61.97, 51.71, 45.15, 41.63, 34.90: anal. calcd; $C_{34}H_{31}N_9O_6$; C, 61.72; H, 4.72; N, 19.05; found; C, 61.94; H, 4.86; N, 19.20.

**4.1.18 7-((1-(2-((4-Methylbenzyl)amino)-2-oxoethyl)-1*H*-1,2,3-triazol-4-yl)methoxy)-*N*-((1-(2-((4-methylbenzyl)amino)-2-oxoethyl)-1*H*-1,2,3-triazol-4-yl)methyl)-2-oxo-2*H*-chromene-3-carboxamide (12r).** Brown solid; yield: 73%; MP = 247–249 °C; IR (KBr, $\nu_{max}$) 3328 (NH), 3055 (C–H aromatic), 2962 (CH aliphatic), 1666 (C=O) cm$^{-1}$; $^1$H NMR (500 MHz, DMSO-$d_6$) $\delta$ 9.08 (t, $J$ = 5.8 Hz, 1H), 8.87 (s, 1H), 8.84–8.70 (m, 2H), 8.27 (s, 1H), 7.98 (s, 1H), 7.93 (d, $J$ = 8.7 Hz, 1H), 7.30 (s, 1H), 7.24–7.02 (m, 9H), 5.33 (s, 2H), 5.18 (s, 2H), 5.12 (s, 2H), 4.60 (d, $J$ = 5.6 Hz, 2H), 4.34–4.20 (m, 4H), 2.38–2.14 (m, 6H); $^{13}$C NMR (126 MHz, DMSO-$d_6$) $\delta$ 165.37, 165.28, 163.14, 161.39, 160.81, 156.08, 148.00, 141.40, 136.10, 136.07, 135.64, 135.61, 131.63, 128.87, 127.38, 126.65, 124.54, 114.75, 114.09, 112.32, 101.09, 63.09, 61.87, 51.64, 42.15, 42.12, 34.82, 20.64; anal. calcd; $C_{36}H_{35}N_9O_6$; C, 62.69; H, 5.12; N, 18.28; found; C, 62.86; H, 5.30; N, 18.40.

**4.1.19 2-oxo-7-((1-(2-oxo-2-(Phenethylamino)ethyl)-1*H*-1,2,3-triazol-4-yl)methoxy)-*N*-((1-(2-oxo-2-(phenethylamino) ethyl)-1*H*-1,2,3-triazol-4-yl)methyl)-2*H*-chromene-3-carboxamide (12s).** Brown solid; yield: 71%; MP = 226–228 °C; IR (KBr, $\nu_{max}$) 3339 (NH), 3032 (CH aromatic), 2866 (CH aliphatic), 1668 (C=O) cm$^{-1}$; $^1$H NMR (400 MHz, DMSO-$d_6$) $\delta$ 9.11 (t, $J$ = 5.7 Hz, 2H), 8.90 (s, 1H), 8.53–8.38 (m, 4H), 8.24 (s, 1H), 8.07–7.89 (m, 2H), 7.34–7.32 (m, 1H), 7.31–7.29 (m, 1H),

7.29–7.27 (m, 1H), 7.24–7.20 (m, 6H), 5.34 (s, 2H), 5.11 (s, 2H), 5.06 (s, 2H), 4.61 (d, $J = 5.6$ Hz, 2H), 3.35–3.21 (m, 4H), 2.80–2.65 (m, 4H); $^{13}$C NMR (101 MHz, DMSO-$d_6$) $\delta$ 165.80, 165.71, 163.63, 161.88, 157.38, 156.58, 148.67, 148.52, 141.84, 141.18, 139.64, 139.62, 132.52, 129.12, 128.85, 128.85, 127.09, 126.66, 124.91, 114.62, 112.90, 72.96, 63.53, 52.08, 40.89, 35.37; anal. calcd; $C_{36}H_{35}N_9O_6$; C, 62.69; H, 5.12; N, 18.28; found; C, 62.85; H, 5.32; N, 18.42.

### 4.2 Cholinesterase inhibitory activity

Butyrylcholinesterase (BChE, E.C. 3.1.1.8, from horse serum), acetylcholinesterase (AChE, E.C. 3.1.1.7, Type V-S, lyophilized powder, from electric eel, 1000 unit), acetylthiocholine iodide (ATCI), butythiocholine iodide (BTCI), 5,5-dithiobis-(2-nitrobenzoic acid) (DTNB) were provided from Sigma-Aldrich for Ellman's test. The cholinesterase-inhibitory activities of all derivatives were assessed using the modified Ellman method as previously reported. Briefly, the synthesized compounds were dissolved in DMSO and diluted in methanol, and 25 μL of the derivatives, 50 μL of the potassium phosphate buffer at pH = 8, and 25 μL of the AChE or BChE were added into each well of the 96-well plates. This plate was incubated for 15 minutes at room temperature. Afterward, 125 μL of DTNB (3 mM in buffer) and ATCI or BTCI were added, and, after 15 minutes, the absorbance at 405 nm was measured.[24,25]

### 4.3 Kinetic study

The inhibitory mode of the most potent compound, **12c**, was investigated against the BChE and AChE enzymes using BTCI or ATCI (0.1–1 mM) as substrates and varying concentrations of the inhibitor.[26,27]

### 4.4 Cytotoxic assay

The cytotoxicity of the most potent analogs was assessed in SHSY-5Y cells using previously reported procedures.[28,29]

### 4.5 Molecular docking

Induced fit docking (IFD) evaluations were performed according to previously reported procedures using the Schrodinger 2018-4 suite. Briefly, the X-ray structures of AChE (PDB code: 4EY7) and BChE (PDB code: 4BDS) were prepared with the Protein Preparation Wizard interface of Maestro by removing the ligand and water molecules, adding hydrogen atoms, optimizing their position, and assigning the ionization states of acid and basic residues according to PROPKA prediction at pH 7.0. The molecular docking was performed using IFD mode.[30] The docking grid was centered on the active site residues defined by the co-crystallized ligand, with a box size of 20 × 20 × 20 Å. Ligands were prepared using LigPrep. For each ligand, 20 poses were generated, and the top-ranking pose based on IFDScore was selected for further analysis. To validate the docking protocol, the co-crystallized ligands were redocked, and RMSD was calculated.

### 4.6 Molecular dynamics simulation

The molecular dynamics simulations for this study of **12c**-AchE and **12c**-BChE were performed using the Desmond v5.3 module (https://www.schrodinger.com/products/desmond) implemented in the Maestro interface (from Schrödinger 2018-4 suite) using the OPLS4 force field. The appropriate pose for the MD simulation of **12c** complexes were obtained by the IFD method. To build the system for MD simulation, the protein–ligand complex was solvated with SPC explicit water molecules. The system was placed at the center of an orthorhombic box of appropriate size under periodic boundary conditions. To reflect physiological conditions, a final concentration of 0.15 M NaCl was used, and appropriate counterions were added both to neutralize the system and to simulate the ionic environment of a real cellular setting. The MD protocol involved minimization, pre-production, and MD simulation steps. In the minimization procedure, the entire system was allowed to relax for 2500 steps by the steepest descent approach. During equilibration, a positional restraint of 5 kcal mol$^{-1}$ Å$^{-2}$ was applied to the protein to prevent drastic structural changes while raising the temperature from 0 to 300 K. MD simulations were performed *via* NPT (constant number of atoms, constant pressure *i.e.* 1.01325 bar, and constant temperature *i.e.* 300 K) ensemble. The Nose–Hoover chain method was used as the default thermostat with a 1.0 ps interval and Martyna–Tobias–Klein as the default barostat with a 2.0 ps interval by applying an isotropic coupling style. Long-range electrostatic forces were calculated based on the particle-mesh-based Ewald approach, with the cut-off radius for coulombic forces set to 9.0 Å. Finally, the system was subjected to MD simulations using the RESPA integrator for 100 ns, with a time step of 2 fs and a box size of 10 Å. During the simulation, every 1000 ps of the actual frame was stored.

The dynamic behavior and structural changes of the systems were analyzed by the calculation of the root mean square deviation (RMSD) and RMSF. Subsequently, the energy-minimized structure calculated from the equilibrated trajectory system was evaluated to investigate each ligand–protein complex interaction.[31]

## Author contributions

S. K. and M. M. synthesized compounds and contributed to the characterization of compounds. A. I performed *in silico* study. M. F. supervised the study. All authors read and approved the final version of the article.

## Conflicts of interest

There is no conflicts to declare.

## Data availability

The author makes their data available upon request from Morteza Farnia.

Supplementary information (SI) is available. See DOI: https://doi.org/10.1039/d5ra09311b.

## Acknowledgements

The authors wish to thank the support of the Vice-Chancellor for Research of Shiraz University of Medical Sciences (grant number = IR.SUMS.REC.1403.452).

## References

1 2024 Alzheimer's disease facts and figures. *Alzheimer's Dement.*, 2024, **20** (5), 3708–3821.
2 2019 Alzheimer's disease facts and figures. *Alzheimer's Dement.* 2019, **15** (3), 321–387.
3 Z. Haghighijoo, S. Akrami, M. Saeedi, A. Zonouzi, A. Iraji, B. Larijani, H. Fakherzadeh, F. Sharifi, S. M. Arzaghi, M. Mahdavi and N. Edraki, N-Cyclohexylimidazo[1,2-a] pyridine derivatives as multi-target-directed ligands for treatment of Alzheimer's disease, *Bioorg. Chem.*, 2020, **103**, 104146.
4 N. Oliyaei, M. Moosavi-Nasab, N. Tanideh and A. Iraji, Multiple roles of fucoxanthin and astaxanthin against Alzheimer's disease: Their pharmacological potential and therapeutic insights, *Brain Res. Bull.*, 2023, **193**, 11–21.
5 M. Yazdani, N. Edraki, R. Badri, M. Khoshneviszadeh, A. Iraji and O. Firuzi, 5,6-Diphenyl triazine-thio methyl triazole hybrid as a new Alzheimer's disease modifying agents, *Mol. Diversity*, 2020, **24**(3), 641–654.
6 A. Iraji, M. Khoshneviszadeh, O. Firuzi, M. Khoshneviszadeh and N. Edraki, Novel small molecule therapeutic agents for Alzheimer disease: Focusing on BACE1 and multi-target directed ligands, *Bioorg. Chem.*, 2020, **97**, 103649.
7 M. Esmkhani, S. Javanshir, A. Iraji and M. Mahdavi, Design and evaluation of substituted cinnamoyl piperidinyl acetate derivatives as potent cholinesterase inhibitors, *Sci. Rep.*, 2025, **15**(1), 19346.
8 H. Pourtaher, A. Hasaninejad and A. Iraji, Design, synthesis, in silico and biological evaluations of novel polysubstituted pyrroles as selective acetylcholinesterase inhibitors against Alzheimer's disease, *Sci. Rep.*, 2022, **12**(1), 15236.
9 A. Rastegari, M. Safavi, F. Vafadarnejad, Z. Najafi, R. Hariri, S. N. A. Bukhari, A. Iraji, N. Edraki, O. Firuzi, M. Saeedi, M. Mahdavi and T. Akbarzadeh, Synthesis and evaluation of novel arylisoxazoles linked to tacrine moiety: in vitro and in vivo biological activities against Alzheimer's disease, *Mol. Divers.*, 2022, **26**(1), 409–428.
10 W. Yao, H. Yang and J. Yang, Small-molecule drugs development for Alzheimer's disease, *Front. Aging Neurosci.*, 2022, **14**, 1–17.
11 M. Saxena and R. Dubey, Target enzyme in Alzheimer's disease: Acetylcholinesterase inhibitors, *Curr. Top. Med. Chem.*, 2019, **19**(4), 264–275.
12 A. Saxena and R. Saini, The structural hybrids of acetylcholinesterase inhibitors in the treatment of Alzheimer's disease: A review, *J. Alzheimers Neurodegener. Dis.*, 2018, **4**, 015.
13 D. Halder, S. Das, R. S. Jeyaprakash and A. Joseph, Role of multi-targeted bioactive natural molecules and their derivatives in the treatment of Alzheimer's disease: an insight into structure-activity relationship, *J. Biomol. Struct. Dyn.*, 2023, **41**(20), 11286–11323.
14 I. Fotopoulos and D. Hadjipavlou-Litina, Hybrids of coumarin derivatives as potent and multifunctional bioactive agents: A review, *Med. Chem.*, 2020, **16**(3), 272–306.
15 K. Bhagat, J. V. Singh, A. Sharma, A. Kaur, N. Kumar, H. K. Gulati, A. Singh, H. Singh and P. M. S. Bedi, Novel series of triazole containing coumarin and isatin based hybrid molecules as acetylcholinesterase inhibitors, *J. Mol. Struct.*, 2021, **1245**, 131085.
16 H. Karimi Askarani, A. Iraji, A. Rastegari, S. N. Abbas Bukhari, O. Firuzi, T. Akbarzadeh and M. Saeedi, Design and synthesis of multi-target directed 1,2,3-triazole-dimethylaminoacryloyl-chromenone derivatives with potential use in Alzheimer's disease, *BMC Chem.*, 2020, **14**(1), 64.
17 Q. Guan, S. Xing, L. Wang, J. Zhu, C. Guo, C. Xu, Q. Zhao, Y. Wu, Y. Chen and H. Sun, Triazoles in Medicinal Chemistry: Physicochemical Properties, Bioisosterism, and Application, *J. Med. Chem.*, 2024, **67**(10), 7788–7824.
18 W. Petrat, C. Wattanapiromsakul, T. Nualnoi, N. H. Sabri, V. S. L. Lee and L. Lomlim, Cholinesterase inhibitory activity, kinetic and molecular docking studies of N-(1-substituted-1H-1, 2, 3-triazole-4-yl)-aralkylamide derivatives, *Walailak J. Sci. Technol.*, 2017, **14**(9), 687–701.
19 S. A. Khan, M. J. Akhtar, U. Gogoi, D. U. Meenakshi and A. Das, An Overview of 1,2,3-triazole-Containing Hybrids and Their Potential Anticholinesterase Activities, *Pharmaceuticals*, 2023, **16**(2), 179.
20 L. Pourabdi, T. T. Küçükkılınç, F. Khoshtale, B. Ayazgök, H. Nadri, F. Farokhi Alashti, H. Forootanfar, T. Akbari, M. Shafiei and A. Foroumadi, Synthesis of new 3-arylcoumarins bearing N-benzyl triazole moiety: Dual lipoxygenase and butyrylcholinesterase inhibitors with anti-amyloid aggregation and neuroprotective properties against Alzheimer's disease, *Front. Chem.*, 2022, **9**, 810233.
21 S. Hosseini, S. A. Pourmousavi, M. Mahdavi and P. Taslimi, Synthesis, and in vitro biological evaluations of novel naphthoquinone conjugated to aryl triazole acetamide derivatives as potential anti-Alzheimer agents, *J. Mol. Struct.*, 2022, **1255**, 132229.
22 S. Zareei, M. Mohammadi-Khanaposhtani, M. Shahali, H. Şenol, M. Badbedast, A. Moazzam, S. Mohseni, E. N. Esfahani, S. F. Ekti, B. Larijani, M. Mahdavi, E. H. Ibrahim, H. A. Ghramh and P. Taslimi, Phenyldiazenyl-phenoxy-1,2,3-triazol-acetamide derivatives as new dual cholinesterase Inhibitors: Design, synthesis, in vitro, and in silico enzymatic inhibition evaluations, *J. Mol. Struct.*, 2025, **1321**, 139686.
23 A. Boobis, U. Gundert-Remy, P. Kremers, P. Macheras and O. Pelkonen, In silico prediction of ADME and pharmacokinetics: Report of an expert meeting organised by COST B15, *Eur. J. Pharm. Sci.*, 2002, **17**(4–5), 183–193.

24 M. Noori, M. Khalili Ghomi, N. Dastyafteh, N. Oliyaei, H. Hamedifar, S. Javanshir, N. Tanideh, E. Sattarinezhad, F. Sattari, M. Haghani, H. Rahmani, B. Larijani, M. Mahdavi, M. H. Hajimiri and A. Iraji, Isoindolinedione-Benzamide Pyridinium Derivatives for Targeting Alzheimer's Disease, *ACS Omega*, 2024, **9**(49), 48032–48043.
25 B. Sadeghian, A. Sakhteman, Z. Faghih, H. Nadri, N. Edraki, A. Iraji, I. Sadeghian and Z. Rezaei, Design, synthesis and biological activity evaluation of novel carbazole-benzylpiperidine hybrids as potential anti Alzheimer agents, *J. Mol. Struct.*, 2020, **1221**, 128793.
26 D. Shareghi-Boroujeni, A. Iraji, M. Dara, M. H. Hashempur, S. Zare, R. Hariri, T. Akbarzadeh and M. Saeedi, Synthesis of novel hybrids of 1,2,3-triazoles-hydrazone: targeting cholinesterases and Alzheimer's related genes, *Future Med. Chem.*, 2024, **16**(15), 1519–1535.
27 S. Loori, H. Pourtaher, A. Mehranpour, A. Hasaninejad, M. Eftekharian and A. Iraji, Synthesis of novel aryl-substituted 2-aminopyridine derivatives by the cascade reaction of 1,1-enediamines with vinamidinium salts to develop novel anti-Alzheimer agents, *Sci. Rep.*, 2024, **14**(1), 13780.
28 H. Pourtaher, M. R. Mohammadizadeh, A. Aliabadi and A. Iraji, The anti-Alzheimer potential of new spirooxindole derivatives containing 1,4-dihydropyridines as a targeted cholinesterase inhibitor, *Results Chem.*, 2026, **22**, 103067.
29 M. Esmkhani, M. Mahdavi, S. Javanshir and A. Iraji, Novel cinnamic acid-based N-benzyl pyridinium analogs: potent dual cholinesterase inhibitors with neuroprotective properties for Alzheimer's disease, *RSC Adv.*, 2026, **16**(10), 9293–9306.
30 S. Loori, H. Pourtaher, A. Mehranpour, A. Hasaninejad, M. Eftekharian and A. Iraji, Synthesis of novel aryl-substituted 2-aminopyridine derivatives by the cascade reaction of 1, 1-enediamines with vinamidinium salts to develop novel anti-Alzheimer agents, *Sci. Rep.*, 2024, **14**(1), 13780.
31 M. Mohammadi-Khanaposhtani, M. H. Sayahi, R. Yazzaf, N. Dastyafteh, M. Halimi, A. Iraji, A. Dadgar, S. Mojtabavi, M. A. Faramarzi and M. Palimi, α-Glucosidase inhibition assay of galbanic acid and it amide derivatives: New excellent semi-synthetic α-glucosidase inhibitors, *Bioorg. Chem.*, 2024, 107580.